Optical Coherence Tomography: 3-D Dental Scanning Imaging Probe

Dubosson Fabrice

February 15, 2007

Contents

List of Figures

Abstract

The principle of Optical Coherence Tomography (OCT) is a based on the light coherence property. OCT generates cross-sectional images of three-dimensional objects. It is non-invasive and often used in the medical field to obtain *in vivo* and *in vitro* images of tissues. This method has been first used in opthalmology, where it gave very good results. Several years ago others medical fields, like: dermatology, cardiology and even dentistry began to use OCT. During these last years, many improvements using new technologies (CCD, swept sources,...) have been done to increase the speed to acquire images (from 8 kHz to 300 kHz), to improve the resolution (from 10 to 1 μm) and to process the visual aspect of the images. The scanning probe field also increased and it appears to be the domain with the most progressive possibilities.

This report describes the development of a three-dimensional scanning imaging probe for the dental domain. In the first chapters, the reader will get familiar with notions about OCT, scanning probes and dental tissues theory. Then a new probe design is described and finally initial measurements are shown and discussed.

Acknowledgments

Special thanks to Professor Zhihua Ding who received me in his laboratory and without who this work would not be possible. Thanks to my Chinese fairy, Jie Meng, who helped me so much. Thanks to all the members of the Ding's laboratory for their kindness and understanding. I really spend a good time in China and I very enjoyed to work with all of them.

Thanks to Mr. GuanMing Lai, Chairman of Seikoh Giken Hangzhou Co., Ltd., for all these interesting conversations and precious ideas.

Thanks to Professor Limin Tong of the Nanophotonics Group for allowing me to use his installations. Special thanks to the Associate Professor Guillaume Vienne for his advice with the optical fibres and the opportunities to speak French.

Many thanks to Professor Martial Geiser for giving me the opportunity to do my diploma work in China and for all his support and advice.

Thanks to every members of the MOVE office to help me with the administrative work.

Thanks to the HES-SO and the HEVs for their generous scholarship.

Special thanks to Mr. Wei Yannian and his team in the mechanical workshop for their incredible work.

Many thanks to everybody I met in China, unknown or not mentioned here, for their help, their support or just their smile when I needed.

Et enfin à vous, papa, maman et Stéphi, merci pour tout!

Chapter 1

Introduction

1.1 The aim of this work

The goal of this work was to built a three-dimensional scanning imaging probe for an optical coherence tomography device adapted to a dental environment [3]. Today the dentists have three possibilities to examine their patients: visual/tactile examination, periodontal probing and radiographic imaging. These methods are invasive and can cause trouble or even be painful. The diagnosis can also be difficult to draw up or can be imprecise. Because the optical coherence tomography technique is non-invasive, has a higher resolution than radiography and can also give information on soft tissue state, it represents a real interesting diagnosis method. The final goal of this probe is trying to help dentists to draw up diagnosis on morphological changes in gingival tissue, tooth decay, and structural integrity of dental restorations.

1.2 Surroundings and Involved People

This work was done at the Optical Engineering State Key Laboratory of Modern Optical Instrumentation of the Zhejiang University according to the agreement between the Haute Ecole Valaisanne (Sion, Suisse) and the Zhejiang University (Hangzhou, China). The supervision was done by professor Zhihua Ding, professor in the Zhejiang University, and the professor responsible to the Haute Ecole Valaisanne was professor Martial Geiser, Industrial Engineering.

When I came in China the theme of my diploma work was nearly defined. I knew I had to deal with optics and something related with embedded systems (programming, electronics, ...). After the precise description of my work I realised that this development called on every knowledges I acquired during my studies: mechanical design, electronic design, power supply and so on... It was enriching to use all these knowledges and to improve them especially in the mechanical field. It also was a real precious experience to work in an foreign country.

1.3 Dental Scanning Probe Overview

This section presents according to the best of my actual knowledge the different developed intraoral handpieces able to give images in two or three dimensions.

The fig. 1.1 shows a probe presented in 1998 by B. W. Colston *et al.* [3] and able to make 2-D pictures. The scanning is done by a DC-motor. The translational motion is perpendicular to the rotation movement of the motor. The fibre is fixed, the GRIN lens and the prism are sticked to the fibre.

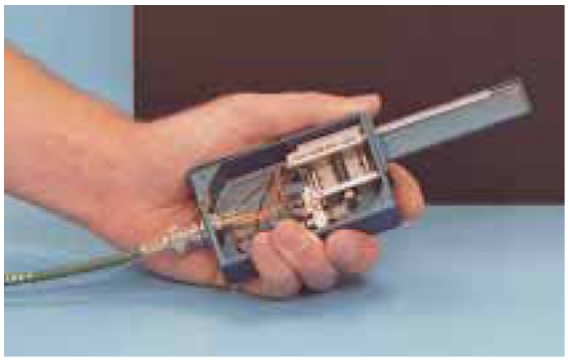

Figure 1.1: Dental OCT Handpiece

Figure 1.2 is a probe used by Evrett *et al.* [10] in 1998. The scanning is also ensured by a DC-motor. The fibre is also fixed and the optical components are sticked together. This probe can also make 2-D pictures.

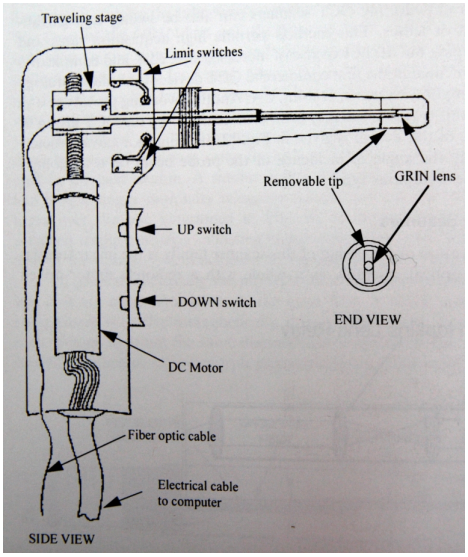

Figure 1.2: Schematic of an hand-held scanner for examination of dental tissues

At least the next figures 1.3 and 1.4 present a probe used by Feldchtein F.I. *et al.* [5] in 1998. This probe is able to make 3-D representation of the sample. The motion is done using electromagnetic principles. The beam is deflecting before the lens and deflected sideway.

Figure 1.3: L-shaped tip of deflecting scanner 1.4 for examination of oral cavity. Bar = 1 cm

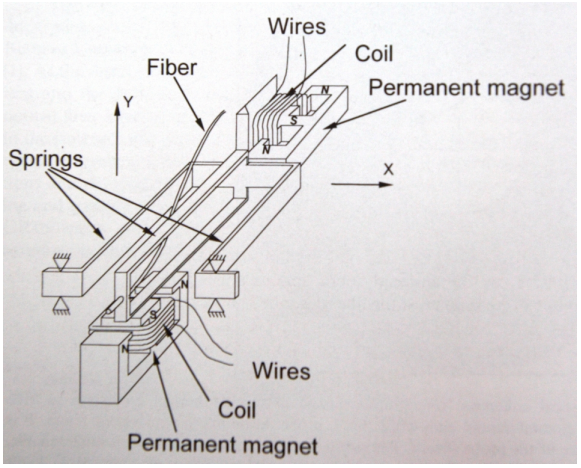

Figure 1.4: Schematic of the deflecting scanner used in the probe fig. 1.3

Chapter 2

Optical Coherence Tomography Theory

The Optical Coherence Tomography (OCT) principle [2] [4] [6] is based on light coherence property to generate cross-sectional images of three-dimensional objects. OCT is non-invasive therefore this technique is often used in the medical field to obtain *in vivo* and *in vitro* images. This method has first been used for a couple of years in the opthalmologic domain where it obtained very good results. Several years ago others medical domains, like dermatology and dentistry, began to use OCT and it is promised to have a great future. Basic knowledges needed to understand the principle of the OCT techniques are explained in the following pages.

2.1 Functioning principle

The principles of an OCT device [2] [4] [6] [9] [11] are mainly related with the interference and the coherence capability of the light.

2.1.1 Optical Interference

One of the light characteristics which is used in the OCT is the phenomenon of interference. Two electromagnetic waves can interfere, add up or subtract each other and create a new one. Interferences could be fully constructive interference or completely destructive (see figure 2.1), but are usually partially descrtuctive or constructive.

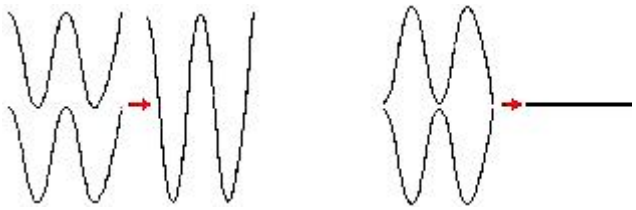

Figure 2.1: Constructive (left) and Destructive Interferences (right)

2.1.2 Spatial and Temporal Optical Coherence

The coherence length describes the time for which the phase of the light wave is known. The daylight has a very short coherent time domain (in order of $\leq 10fs$). On the contrary the laser light has a very high coherence domain (in the order of $\geq 1ps$). Many applications need a high coherent light source but OCT make use of a low coherent light source (in the order of $50fs$) such a superluminescent diode (SLD, diode between a standard light emitting diode (LED) and a laser diode). The coherence time domain τ is given by dividing the coherence length by the phase velocity of light in a medium; or approximatively given by $\tau = \frac{\lambda^2}{c\Delta\lambda}$. Where λ is the centered wavelength, $\Delta\lambda$ bandwidth of the light source and c the speed of light in vacuum. The coherence time also determines the axial resolution (see 2.2.1 eq. 2.1 on page 8).

Figure 2.2 shows the differences between a laser which is nearly monochromatic and a SLD which has a larger bandwidth. It is to be noted that the coherence length is inversely proportional to the bandwidth. If two waves with the same frequency and a finite duration t built an interference, it means that the delay time Δt between the two waves is smaller than t. In this case the two waves are temporally coherent.

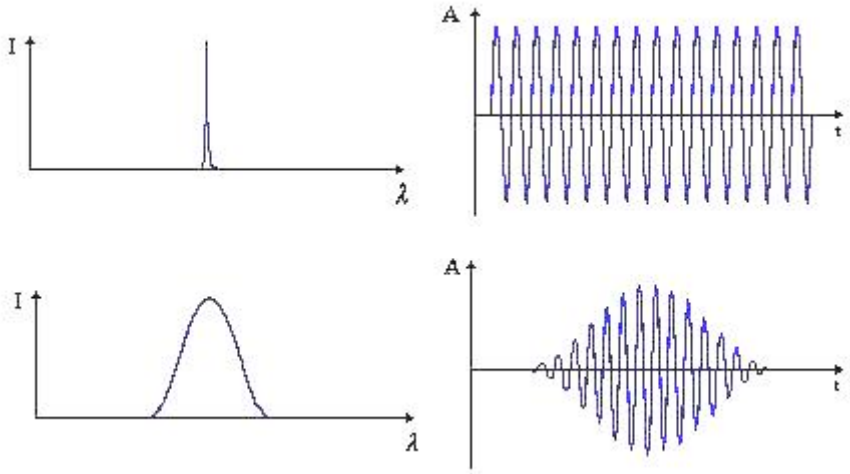

Figure 2.2: Laser Coherence (above) and Superluminescent Diode Coherence (below). The two figures on the left describe the spectrum of the two different light sources (X-axis is the wavelength, Y-axis is the intensity) and those on the right side show the coherence of these two sources (X-axis is time, Y-axis is the amplitude)

The spatial coherence describes the correlation between waves at different points in space. This effect is dependent on the size of the light source (shining part) and on the correlation of beams which originate from different points of the surface of the light source. With lasers and SLD's the spatial coherence is larger than the daylight or a conventional lamp and the temporal coherence is the most important effects but the spatial coherence has not to be neglected.

2.1.3 Simple OCT System

The interferometric technique using a low temporally coherent light source is named Low Coherent Interferometry (LCI). It allows to measure absolute movement in contrary to classical interferometry which analyze relative moving. This is the technique used in OCT system to build images. This property is used to measure the depth origin (axial) of the back scattered or reflected light. Figure 2.3 shows the principle of a Michelson interferometer and 2.4 describes a simple fibre-based time-domain optical coherence tomography system.

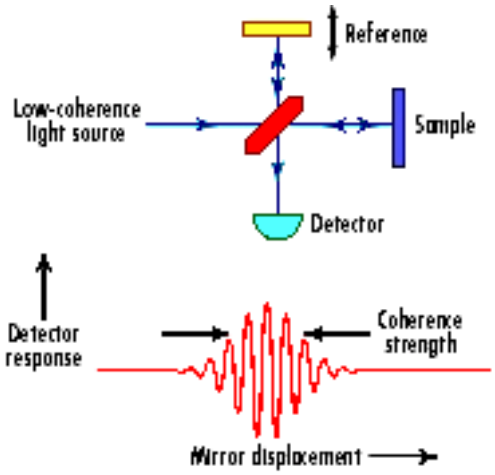

Figure 2.3: Interference Principle in a Michelson Interferometer

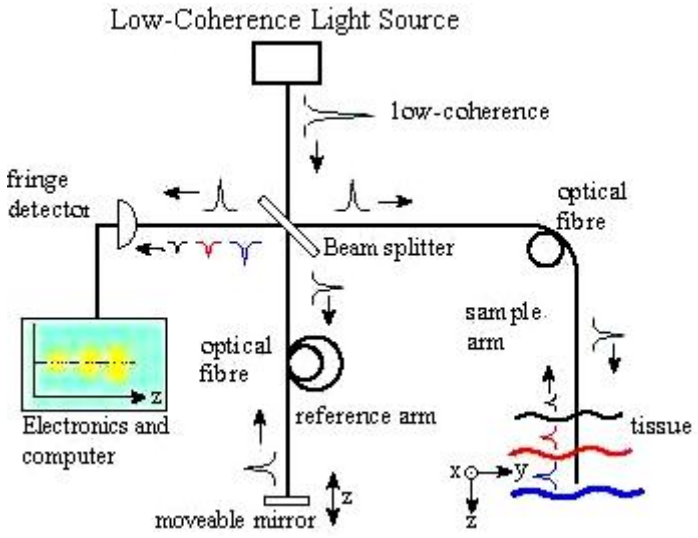

Figure 2.4: Schematic of the OCT System

The light source has low-coherence like an SLD. Light is driven through the fibre to the beam splitter which divide by two (50/50) the beam. The first 50% are driven in direction of the sample (sample arm) to be reflected or backscattered by the different sample's tissues. The second 50% go through the reference arm ended by a movable

mirror. Both are reflected back to the detection arm which has a detector to convert light intensity into electrical current. That current is converted to a digital signal and analyzed by a computer which generates an image of the sample. Interference fringes can only appear if both optical path length of the sample arm and reference arm are strictly the same to within about the coherence length (fig. 2.3). Moving axially the mirror of the reference arm change the optical path length, this motion make therefore a depth scanning (Z-axis) of the sample. Note moreover the lateral scan (Y-axis or X-axis) has to be performed by moving the sample or by scanning the probe beam illuminating the sample to obtain a two-dimensional (2-D) sample's picture. To do a three-dimensional (3-D) sample's representation every axis (X,Y,Z) have to be scanned.

2.2 Resolution

An interesting aspect of the OCT techniques [2] [4] [6] [9] [11] is that the resolutions are independent. This fact allows to design a specific scanner for each scanned axis in each application.

2.2.1 Axial Resolution

The axial resolution (depth resolution, resolution on the Z-axis) depends on the coherence length of the light source. So a high axial resolution can be achieved independently of the beam-focusing conditions. Equation 2.1 gives the axial resolution Δz for a light source with a Gaussian spectral distribution:

$$\Delta z = \frac{2ln2}{\pi}\left(\frac{\lambda^2}{\Delta\lambda}\right) \tag{2.1}$$

where Δz and $\Delta\lambda$ are the full width at half-maximum of respectively the autocorrelation function and power spectrum. λ is the center wavelength of the light source. As written before, is that the axial resolution is inversely proportional to the bandwidth. Therefore a high resolution is obtained with a broad-bandwidth low-coherence light source. The very large bandwidth of the sun or of a white-hot lamp seems to be a great solution but their spatial coherence is not satisfactory.

2.2.2 Transverse Resolution

The transverse resolution (axis X and Y) for OCT obeys the same laws than classical optical microscopy and depends on the focusing properties of an optical beam. The equation 2.2 determines the transverse resolution(X or Y axis):

$$\Delta x = \Delta y = \frac{4\lambda}{\pi}\left(\frac{f}{d}\right) \tag{2.2}$$

where f is the focal length of the objective lens and d the beam size diameter on the lens. To achieve a high resolution a short focal length and a large beam diameter are needed. However transverse resolution and depth of focus (DOF) or confocal parameter b (eq. 2.3) are related to the Rayleigh length z_R (eq. 2.4) by:

$$b = 2z_R \tag{2.3}$$

$$z_R = \frac{\pi \Delta x^2}{4\lambda} \tag{2.4}$$

This relation means that a high resolution implies a small depth of field. The same phenomenon is found in conventional microscopy. The numerical aperture (NA), of a lens or an optical system, is defined by: $NA = n \sin u$ where n is the refractive indice of the image medium and u the angle between the marginal ray and the optical axis. The figure 2.5 illustrates different depths of field for a large and a small NA.

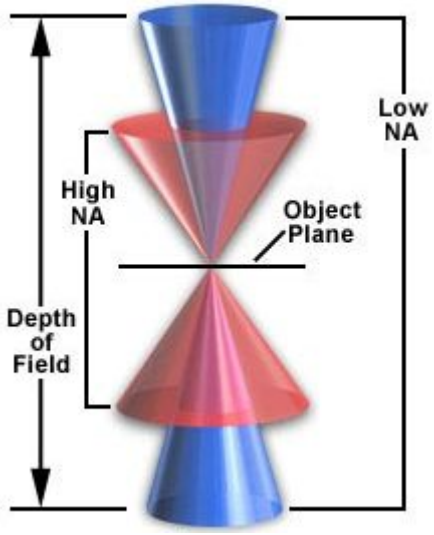

Figure 2.5: Depth of Field

During the optical conception a compromise has to be reached related to the aim of the designed system. A low NA allows to obtain a large depth of focus at the expense of the transverse resolution. In choosing this possibility the confocal parameter is larger than the coherence length ($b > \Delta z$), the axial resolution depends on the coherence length and the transverse resolution on the spot size. A possibility to reach a high transverse resolution and keep a depth of focus sufficient is to do a focus-tracking. The focus-tracking is a dynamic adaptation of the focal length during the scanning process. However this method could lead to a complex development. On the other hand it is possible to work with a high NA to increase the transverse resolution. In this case the confocal parameter can be shorter than the coherence length of the light ($b < \Delta z$). This solution is implemented to differentiate backscattered or backreflected light from different depths. This method is called optical coherence microscopy (OCM).

Chapter 3

Scanning Systems Theory

As described in 2.1.3 to obtain images in two or three dimensions [4] [9], it is necessary to scan the sample. The scanning system is a complex part of an OCT device and the following chapter is focused on this specific subject of the OCT technique.

3.1 Optical System

The optical system is used to focused the beam on the sample and collect the light back-scattered or reflected from the sample back to the interferometer. For OCT based on single-mode fibre the optical system also relays the fibre tip image with a magnification to the sample. This magnification is a compromise between the transverse resolution and the depth of field (see 2.2.2). Generally, to provide acceptable image quality, aspherical or GRIN lens or even microscop objective are used but size and cost may play a role in the choice of the optical system.

3.2 Mechanical System

The aim of a mechanical system is to sweep the focused beam across the region of interest. The main requirements for a scanner are size (see 3.3), scanning rate and safety. But depending on the use of the probe other requirements can be added like shape, convenience in application, sterilizability or weight.

The mechanical system must moreover be able to move the beam on the entire desired surface and to keep the transverse resolution obtained by the optical system. Therefore the mechanical resolution has to be at least twice smaller than the optical resolution.

The scanning rate, frame per second (fps), related with the scanning speed is important too. There are virtually no limitations to the scanning speed and there is no clear ultimate values of scanning rates for different scanning methods. The speed and by the same way the scanning rate have to be fixed according to the acquisition rate which represents the only barrier. Note that faster the scanning is done, less motion artifacts (artifacts produced by the movements of the patient) will appear.

3.3 OCT Scanners Sizes

The OCT scanners can be classified in three different sizes: bench top, hand-held and endoscopic.

The benchtop size is a scanner with virtually no space limitations often use in research laboratories or applications where scanner size is not critical.

The hand-held scanner is the middle size. It is used where the available space is of the order of several tens of cubic centimeters. These limitations already complicate its development.

At least the smallest size is the endoscopic one. The endoscopic scanners are used in applications where the available space is of order of or less than 1 cm^3. Especially in the medical field where *in vitro* pictures are required. Its very small size make its design inevitable demanding in the choice of its components.

3.4 Scanning protocols

The idea of an OCT scanner is to move either the sample or the probe beam to cover the whole region of interest. Generally the sample is not moved due to practical reasons. There is several scanning protocols related to the imaging engine and the application. Cross-sectional images can be obtain using either the depth- or transverse-priority respectively A- and B-scan.

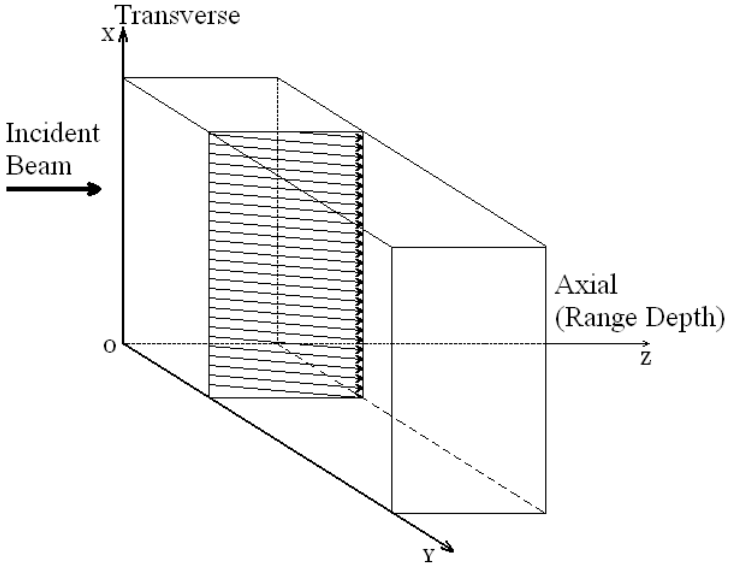

Figure 3.1: Depth Priority Scanning Protocol, A-Scan

Figure 3.1 shows the depth priority scanning. The Z-axis is scanned quicker than the transverse X-axis. The implementation of the Z-axis scanning engine can be done outside the probe that makes its conception easier. The transverse scanning design for an A-scan protocol is also easier to think. However no focus-tracking can be done with a depth priority protocol.

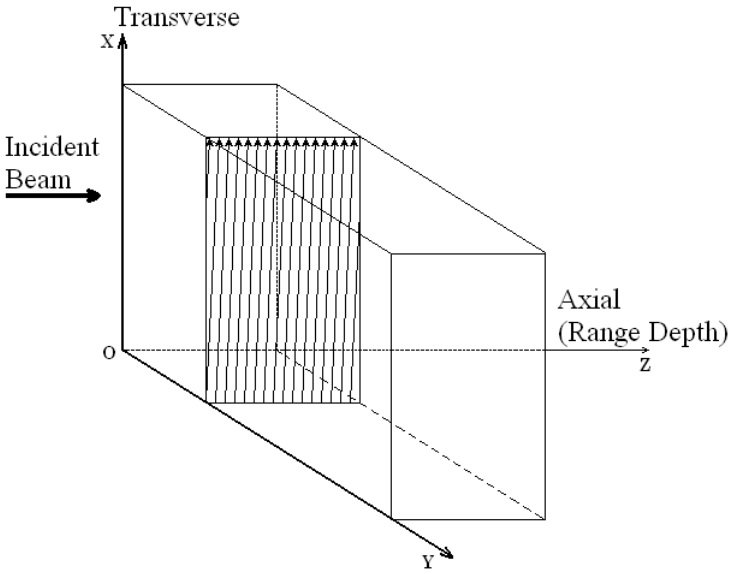

Figure 3.2: Transverse Priority Scanning Protocol, B-Scan

Picture 3.2 represents a B-scan protocol. The transverse axis (X or Y) is scanned faster than the depth one. Here the possibility of a focus tracking exists. Generally the design of the lateral scan element is more complex.

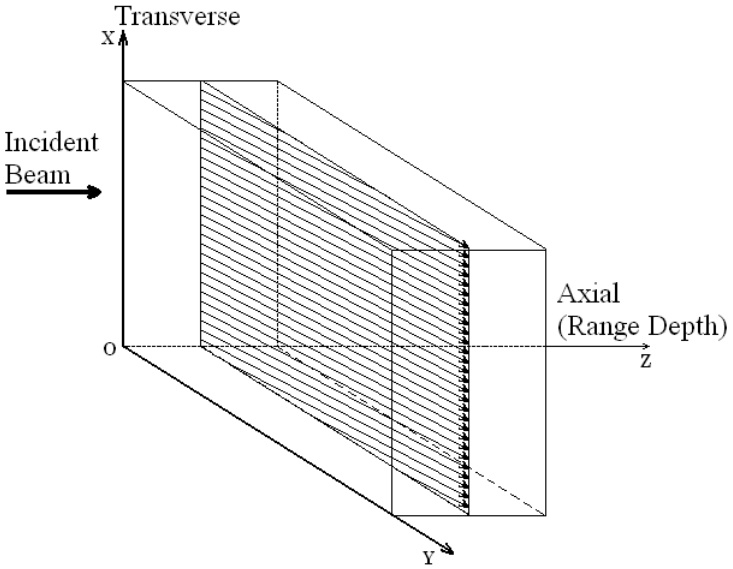

Figure 3.3: Transverse-priority in Two Dimensions, *en face* images

If the two transverse axis (X and Y) are scanned before the axial one (Z), *en face* images are obtained at a given depth (Figure 3.3).

To get three-dimensional pictures, several images obtained with one of this scanning protocols are stacked. The picture 3.4 shows the 3-D imaging principle using the A-scan protocol. The resolution between two cross-sectional images depends on the same characteristics than the transverse resolution (refer to 2.2.2 on page 8) and, of course, on the step ability of the scanning engine.

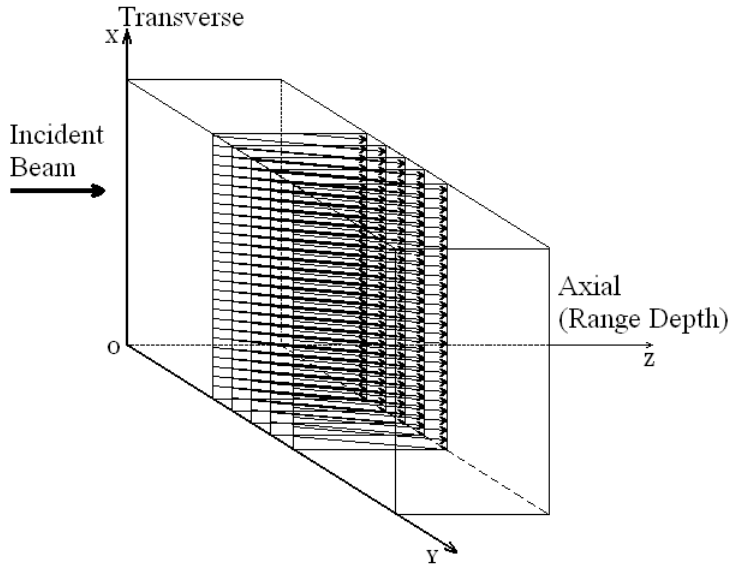

Figure 3.4: 3-D Image with the A-Scan Protocol

3.5 Scanning Directions

Two directions can be chosen to ensure the scanning: forward-looking and sideways-looking. The choice will depend on the available space, the sample's nature(e.g. blood vessels or organs), the use of the probe (e.g. *in vitro* or not) and the position of the interest zone from the scanning probe. Figure 3.5 demonstrate the two possible scanning directions.

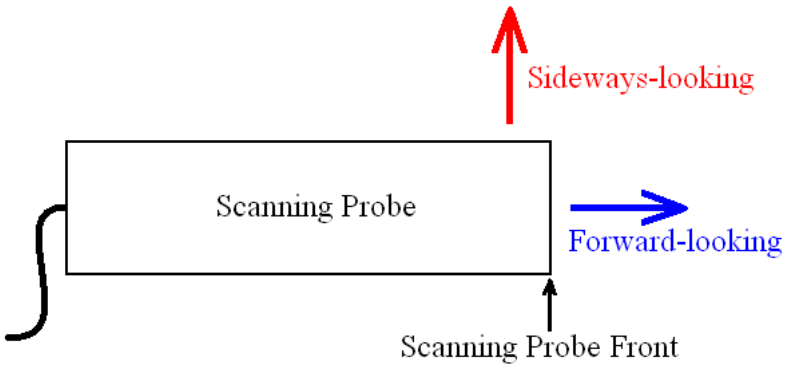

Figure 3.5: Sideways-looking and Forwards-looking Scanning Directions

3.6 OCT Scanners Implementations

There are three possibilities of OCT scanners implementation: circumferential, deflecting or translational. The solution has to be defined according to the aim of the scanning probe and its environmental use.

3.6.1 Circumferential Scanners

The principle is to rotate the beam in the plane transverse to the instrument (fig. 3.6). This kind of implementation cannot be done with an forwards-looking scanning direction due to its own nature. The image representation is in polar coordinate but can be reconstructed in orthogonal coordinate by computer processing. Note that the physicians are already used to read images in polar coordinate with ultrasonography. This scanner implementation is suitable for examination of organs with a narrow lumen, especially for intravascular imaging and narrow ducts in urinary or low respiratory systems.

Figure 3.6: Circumferential Scanning Probe Implementation

3.6.2 Deflecting Scanners

In a deflecting scanners (fig. 3.7) a mechanism deflect the beam before its incident on the focusing system (principle of beam motion). This deflection can also be oscillations. The beam can moved 1-D or 2-D along an arbitrary trajectory in the transverse plane. A deflecting scanner can be implemented in sideways or forwards-looking direction depends on its purpose. The image representation of this scanner type is orthogonal. This kind of scanners are superior for *en face* imaging and suitable for 3-D image acquisition.

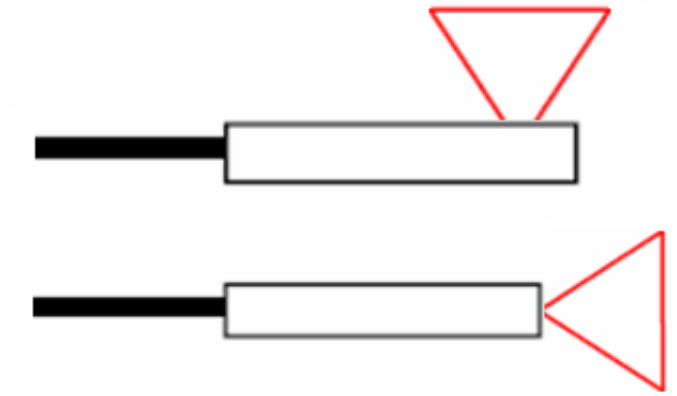

Figure 3.7: Deflecting Scanners, above sideways-looking and below forwards-looking

3.6.3 Translational Scanners

The scanning is caused by the linear translation of the optical system itself while the beam position relative to the optical components remains invariable (fig. 3.8). The image representation is orthogonal. These scanners are convenient for covering large surface area with minimal geometrical aberration of acquired images.

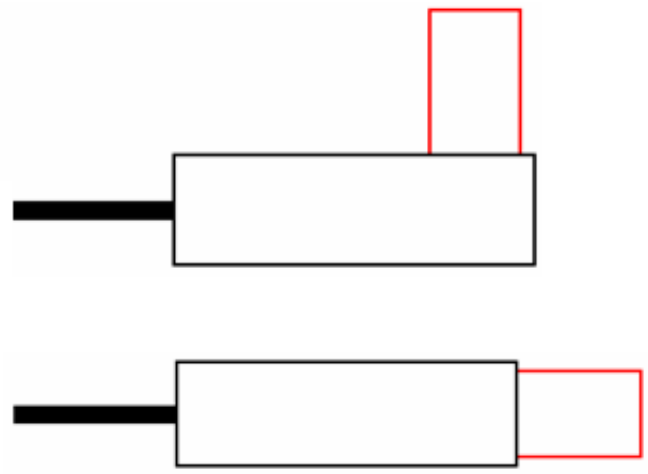

Figure 3.8: Translational Scanners, above sideways-looking and below forwards-looking

Chapter 4

Dental tissues Theory

4.1 Tooth Anatomy

Figure 4.1 shows the cross-sectional anatomy [3] [4] of a normal tooth.

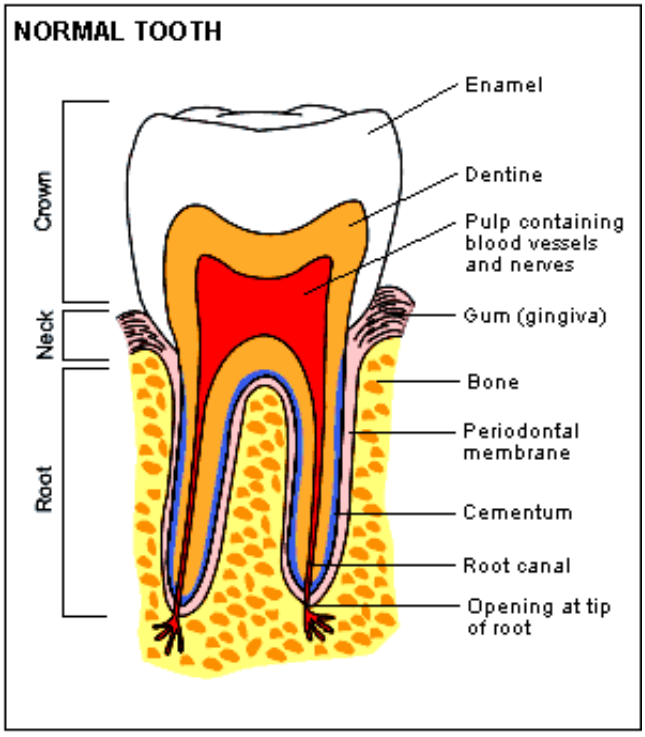

Figure 4.1: Tooth Anatomy

The enamel layer is made up with hydroxyapatite crystals prisms (fig. 4.2). They can have a length of 3 - 4 mm near the cervix of the tooth and a mean diameter of 6 μm. These prisms which look like a car tyre section are separated by a glycoprotein prism sheaths 0.1 - 0.2 μm wide.

Under the enamel layer is the dentin. This is a complex structure where dentinal tubules are placed like honeycombs in a collagen matrix. The tubules are composed of long cell processes (ondontoblasts) and surrounded by small hydroxyapatite crystals needle-like (1 - 3 μm in diameter) in a fibrous matrix (type I collagen fibres).

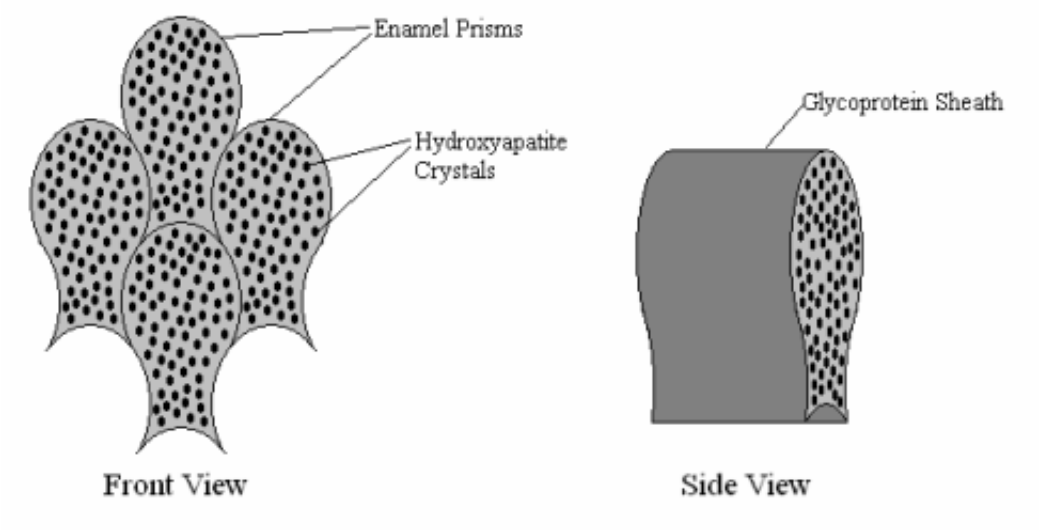

Figure 4.2: Structure of Enamel Prisms

The neck is the beginning of the periodontium. This is made of several kinds of basic tissues. The superficial one is an epithelium which cover and protect the underlying tissues. Under the epithelium is the periodontal ligament. [1] This ligament is a specialized connective tissue that attach teeth from the cementum to the surrounding alveolar bone. The small space between the epithelium and the tooth in the neck area is the sulcus and this is an important place to detect periodontal disease.

4.2 Optical Properties of Dental tissues

The hard tissues are anisotropic therefore the scattering distribution is highly orientation-dependent. Studies show that the average scattering coefficient (μ_s) for enamel varies significantly with the wavelength ($\mu_s(632nm) = 60cm^{-1}, \mu_s(1053nm) = 15cm^{-1}$). In comparison the dentin scattering coefficient is less dependent on the wavelength ($\mu_s(632nm) = 280cm^{-1}, \mu_s(1053nm) = 260cm^{-1}$). For both hard tissues the absorption coefficient (μ_a) can be neglected. The indexes of refraction are at $\lambda = 633nm$ approximately 1.63 for enamel and 1.45 for dentin. About the soft tissues no study, to the best of my knowledge, have be done for measuring the optical properties.

Chapter 5

Scanning Probe Design

5.1 Time Domain OCT Device Descritption

The following fibre-based OCT device has been implemented in the professor Zhihua Ding's Laboratory in Optical Engineering State Key Laboratory of Modern Optical Instrumentation of the Zhejiang University. The schema 5.1 shows the main elements composing the system. The detailed information are listed in appendix B.

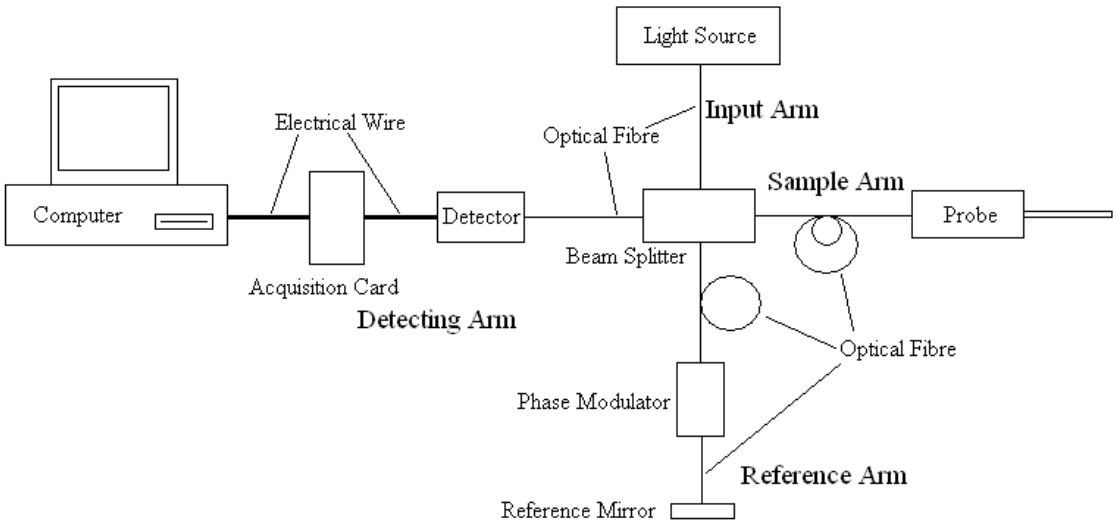

Figure 5.1: OCT System

5.2 Scanning Probe Concept

The requirements for this probe were the followings:

- three-dimensional dental scanning imaging probe;
- scanning area: 6 mm by 3 mm;
- resolution: at least 15 μm on every axis.

Additional requirements:

- sterilizability;
- safety;
- convenience in application for the physician;
- comfortable for the patient;
- affordable.

After considering all these requirements and the study of diverse patents and articles, it has been decided to develop an hand-held sideways-looking scanning probe which has two different scanning technologies. (Appendix A). Figure 5.2 shows the general concept of the scanning probe design. The axial scanning (Z-axis) is done by the OCT device with the galvanometer therefore this axis has not to be considered in the scanning probe design. The scanning on the Y-axis is ensured by the DC-Motor which rotates the screw to

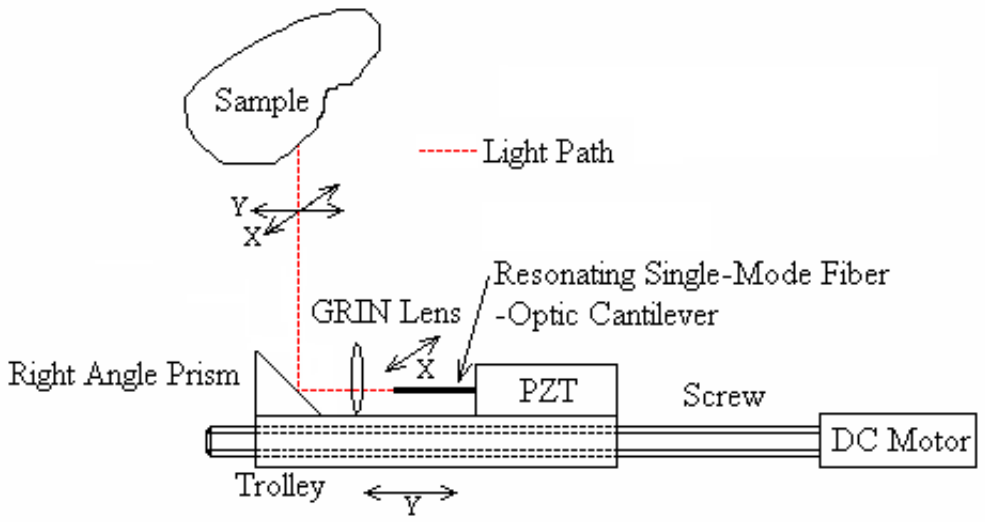

Figure 5.2: General Concept of the Scanning Probe

displace the trolley forward or backward (translational scanner). The X-axis is scanned using a piezzo electrical element which put a single-mode optical fibre cantilever in a resonating mode (deflecting scanner).

5.3 Mechanical Design

The mechanical part is the skeleton of the probe. It must carry, move and protect the other parts. Appendix I contents the drawings of the mechanical parts machined by the Zhejiang University Mechanical Workshop.

Figure 5.3: the motion is produced by a DC-motor which rotate a screw. The rotation movement is transformed in a translation motion by the trolley which also support the optical components.

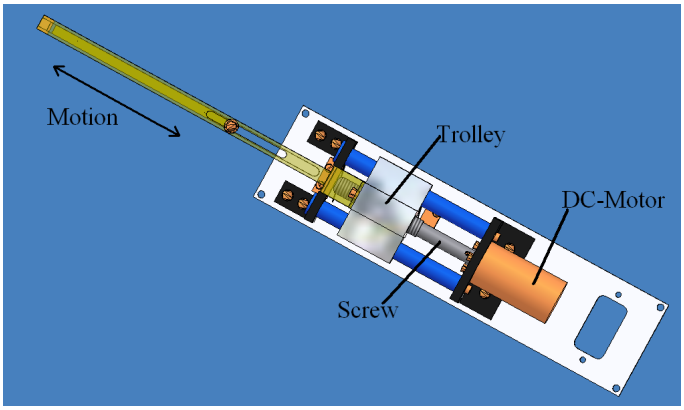

Figure 5.3: Motion and Optics Support

The DC-motor (appendix D, Nb. 110078) is assembled with an encoder (appendix E, Nb. 201940) which gives 512 ticks per motor's revolution. These ticks are received by a positioning control unit (appendix F, EPOS 24/1) which is able to drive electronically the motor like a stepper motor. The positioning control unit receives the orders from the computer via a serial port RS 232. Two end-switches are fixed to set the position of the trolley before the measuring.

The screw has a pitch of 1 mm that means when the screw does one revolution, the trolley moves from 1 mm forwards or backwards depending on the direction of rotation. The system: screw, trolley, DC-motor-encoder and positioning control unit, reaches theoretically a precision of 2 μm. This precision is five times less than the required precision (10 μm) and therefore satisfies the sampling theorem.

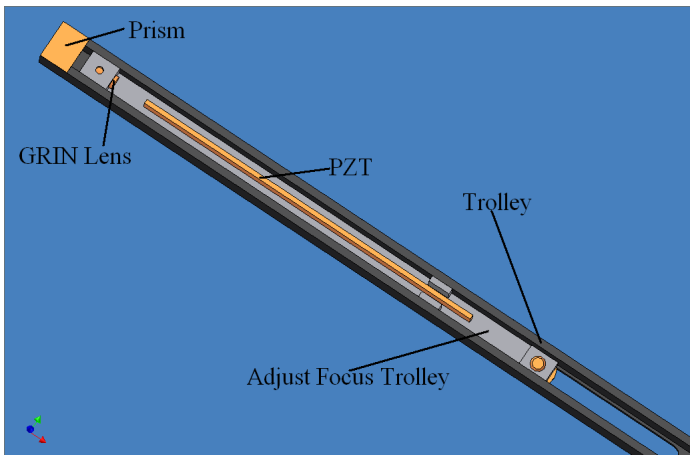

Figure 5.4: Detail of the Scanning Probe Head

Figure 5.4: a small trolley allows to set by hand the depth of the focus point in the sample in modifying the length of the optical path from the end of the GRIN lens to the prism. This trolley also supports the piezzo bilaminar element.

The piezzo element (appendix G) is a piezzo ceramic bilaminar strip actuator (fig. 5.5). On this element is sticked the optical fibre cantilever. When sinusoidal waves of opposite polarities are applied to the electrodes, the strip actuator will bend transversely

and the optical fibre cantilever will be displaced along with the bilaminar element. As the sinusoidal wave frequency matches the mechanical resonance of the cantilever, the transverse displacement of the fibre cantilever reaches a maximum [12].

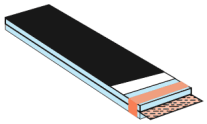

Figure 5.5: Strip Actuator

The resonance frequency of a round cross-section cantilever (here the optical fibre) is given by [8]:

$$f_r = \frac{\beta}{4\pi}\sqrt{\frac{E}{\rho}}\left(\frac{R}{L^2}\right) \tag{5.1}$$

where L and R are respectively the length and the radius of the cantilever, E the Young's modulus, ρ the mass density and β is a constant determined by the vibration mode number and boundary conditions of the cantilever. Here $\beta \cong 3.52$ because the zeroth order vibration mode is used. According to the possible acquisition rate of the detector a resonance frequency of 2.5 kHz, corresponding to a scanning rate of 5 kHz, has been chosen. This frequency involves for an average $\cong 20$ μm optical fibre radius, a cantilever length of 3.57 mm. For the calculation $E = 7.17 \cdot 10^{10}$ Pa and $\rho = 2.2 \cdot 10^3 kg/m^3$, which are values of the silica (Appendix: H), have been used. The single-mode optical fibre is a standard telecommunication single-mode fibre (see 5.7) which was stretched to reach a core diameter of 3 μm and an outside diameter of 40 μm.

All the system has been embedded in an housing to protect the scanning system (optical and mechanical parts) and to allow an easy handling. The picture 5.6 shows the mechanical pieces of the scanning probe prototype bare mounted without the bought components (switches, DC motor, strip actuator,...).

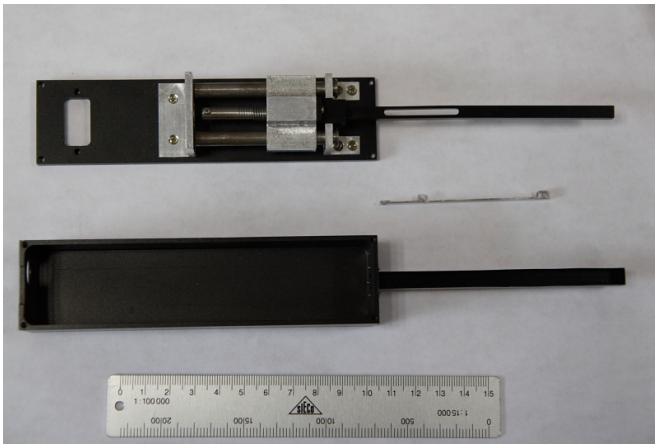

Figure 5.6: Mechanical components, ruler = 15 cm

5.4 Optical Design

The optical design (fig. 5.7) is based on three components: the optical fibre, the gradient index (GRIN) lens and the right-angle prism. The concept is to put the optical fibre in a resonance mode with an amplitude of 1 mm. The fibre oscillations will do a line which will be the object of the optical system. This object will be casted on the sample through the lens and the prism with the aim of being reflected or backscattered and therefore give the informations of the sample.

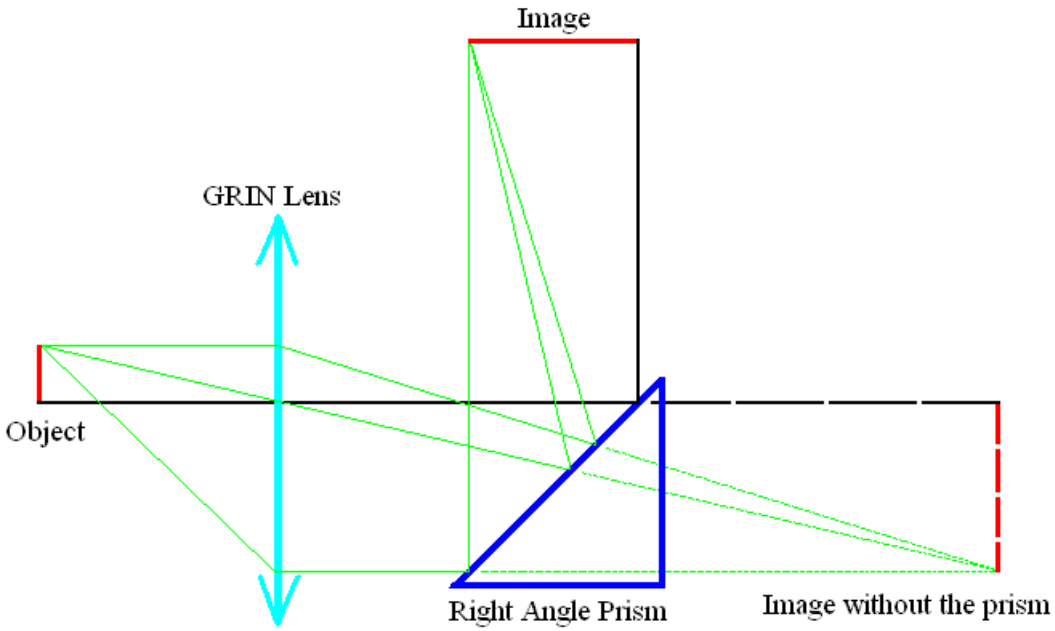

Figure 5.7: Optical Design Principle

Note that no imaging quality calculation have been done.

5.4.1 Gradient Index Lens

Figure 5.8 shows the principle of a GRIN lens. Using a radially-decreasing refractive index (usually a parabolically shaped index profile) the light beams are deflected, their path become sinusoidal inside the lens, and after could converge like with a normal converging lens. Actually a GRIN lens behaves like a standard lens but is not shaped the same. Therefore this type of lens is used where many very small lenses are needed to be mounted together. They are also used in the telecommunication field to couple two fibres together, to collimate a beam after an optical fibre or to focus a laser beam in an optical fibre. One of their biggest advantage is their shape (like tube) which allowed an easier use than a traditional lens shape.

For a GRIN lens, the transverse linear magnification is given by [7]:

$$M_t = \frac{x_2}{x_1} = \cos\Delta - \frac{n_0}{n_2}\frac{z_2}{L}\sin\Delta = \left(\cos\Delta + \frac{n_0}{n_1}\frac{z_1}{L}\sin\Delta\right)^{-1} \tag{5.2}$$

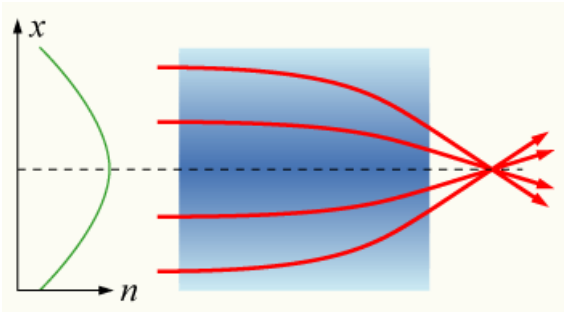

Figure 5.8: Typical GRIN Lens

where x_1 and x_2 are respectively the size of the object and the size of the image. n_0 is the refractive index of glass in the middle of the lens, n_1 and n_2 are the refractive indexes from the object medium and the image medium respectively. z_1 is the distance between the object and the first face of the lens and z_2 is the distance from the second face of the lens to the image. At last, $\Delta = \frac{D}{L}$ where D is the diameter of the lens and $2\pi L$ is the total lens length with a pitch of 1. The pitch is an important characteristic of a GRIN lens. A pitch of 1 means that the light rays are doing a complete period (2π) inside the lens. For instance a pitch of 0.25 is a quarter of a period ($\frac{\pi}{2}$), 0.5 is an half period (π) and so on. Common used pitch is 0.23 and 0.25 but a custom pitch can be done quite easily in changing the length of the lens. Appendix C gives the used GRIN lens characteristics.

For this probe a magnification of -3 has been chosen as compromise between the optical fibre diameter and the positions (working distances) of the image (z_1) and the object (z_2). The following values have been calculated, z_1 = -0.889 mm and z_2 = 6.05 mm.

5.4.2 Right Angle Prism

The right-angle prism is a standard glass BK7 prism. Its function is to deflect the beam in the sideways direction. It behaves like a mirror but due to its shape, its use is easier. The prism has simply been sticked on the mechanical part.

5.4.3 The Optical Fibre

The optical fibre is a standard telecommunication fibre for a wavelength of 1300 nm. It is stretched by hand to obtain a diameter of nearly 3 μm to reach the 10 μm precision requirement. Its outside diameter is about 40 μm wide. The procedure to stretch an optical fibre is the following. First the outside jacket in polymer is taken off from the fibre with a special tool. After the bared fibre (core and cladding) is cleaned with ethanol to remove the last rest of polymer. At least the fibre is put over a flame and subject to a light traction. Due to the heat the glass of the fibre will became pasty and will let it stretch easily. The picture 5.9 shows the head of the stretched optical fibre.

A stretched single-mode optical fibre will have more losses but the NA will nearly remains the same. The biggest change is the fragility of the fibre which has to be handled carefully.

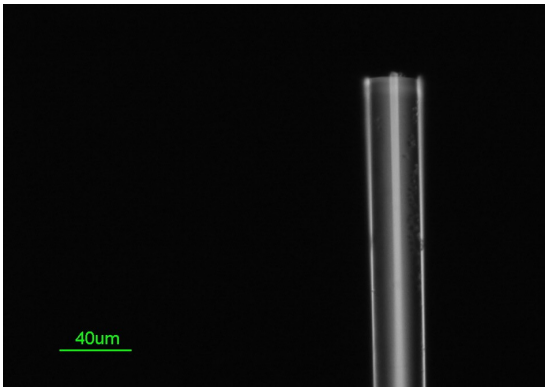

Figure 5.9: Stretched Optical Fibre Tip

Note that to have an easier handling the fibre is sticked on the piezzo element without the connector. A second fibre with a connector is welded to the first one at the end of the assembly.

5.5 Design Conclusion

According to the mechanical design the transverse resolution obtained with the DC motor would reach 10 μm with a range of the order of 1 cm. On the other axis the range would reach 3 mm with also a 10 μm resolution. The depth of field of the optical system would be $\cong$ 120 μm in free space (see eq.: 2.3 and eq.: 2.4 with λ = 1310 nm and Δx = 10 μm). These forecast fulfill the requirements.

After comparison with the existing probes (see 1.3), this design is actually the first design of a 3-D dental scanning imaging probe using two different technologies (DC motor and strip actuator) and implementations of OCT scanners (deflecting and translational) at the same time.

Chapter 6

Results

6.1 Mechanical Axis

The tests on the mechanical axis with the DC motor, the screw and the switches could not be done. At the time of the first tests on the motor and the controller alone, after the configuration of the computer was done, the encoder was burnt. The present report can *de facto* not give any results for this scanning axis.

6.2 Bilaminar Axis

For these measurements the system comprises the fiber cantilever, the GRIN lens, the piezzo element and the support (fig. 6.1). In the following part it will be called the probe.

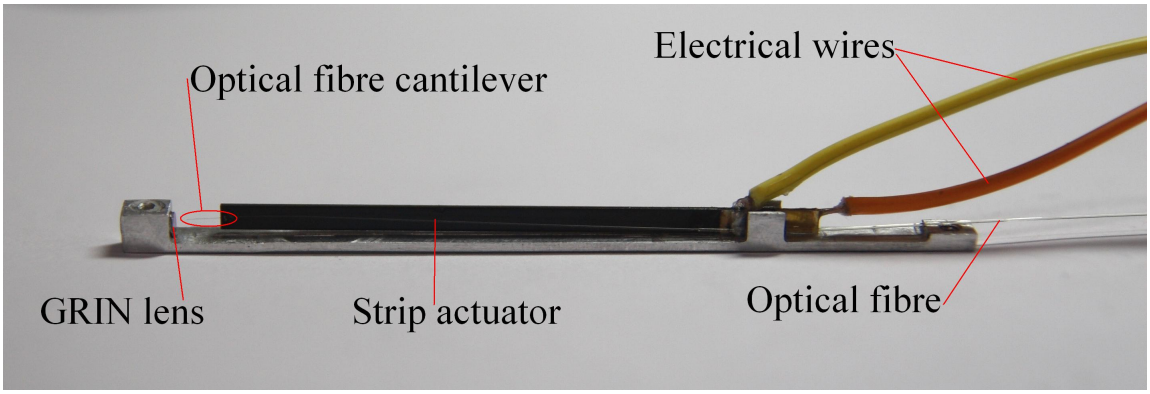

Figure 6.1: Tested System

The used instruments are listed in appendix B.

6.2.1 Resonance Frequency

To find the resonance frequency f_r a sinusoidal signal with an amplitude of 20 V and frequencies from 10 Hz to 3 kHz with 10 Hz step was applied on the piezzo element. The amplitude of the beam deflection was measured on a graduated target (ruler) placed at 3 cm of the GRIN lens last face.

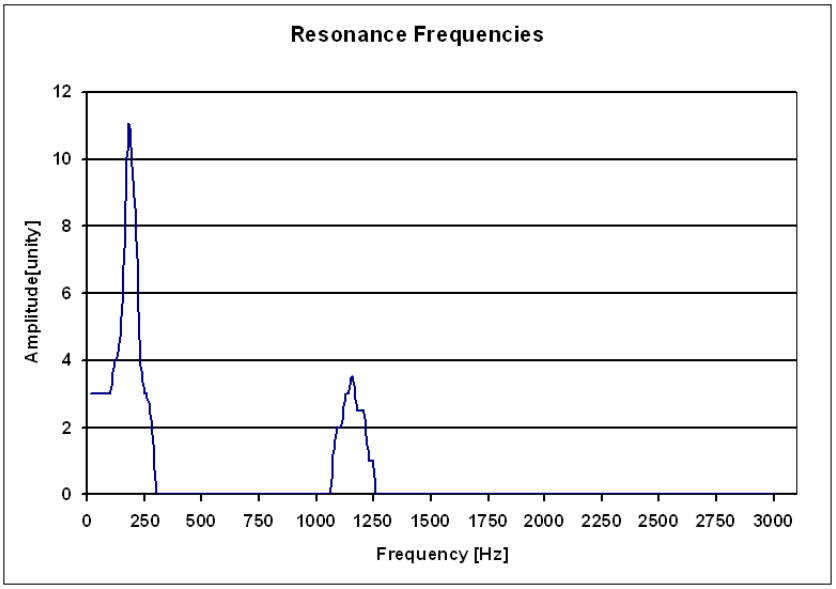

Figure 6.2: Half Fixed Sample Resonance Frequencies

The diagram 6.2 shows the amplitude behavior of the deflected beam. First the system is fixed backwards.

Diagram 6.3 shows the same measures but this time the system is fixed backward and frontwards.

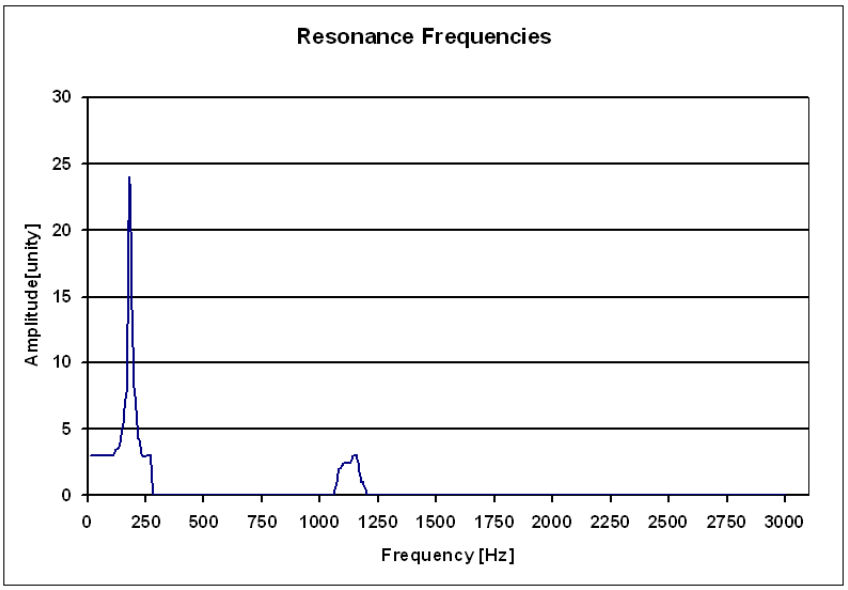

Figure 6.3: Total Fixed Sample Resonance Frequencies

The two maximums are in the same frequencies on both diagrams, the first at **180 Hz** and the second at **1160 Hz**.

6.2.2 Interferences Capability

To test the capability of the probe to deliver and catch the reflected light from the sample, the probe was plug in the OCT system and the sample was a mirror.

The first short observation shows that the spot from the fibre tip is very speckled.

To obtain interference fringes the sample has to be placed at the focal distance of the lens. This distance has been measured and its value is ≅**6 mm**.

Figure 6.4 represents the signals displayed on the oscilloscope. The yellow signal is the signal received by the light detector in the detecting arm. Interference fringes can be seen in the ellipse.

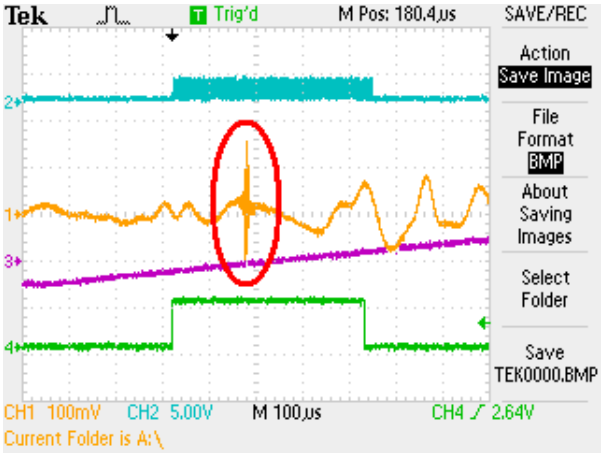

Figure 6.4: Interference Fringes

On figure 6.5 the same signal is displayed with a smaller time scale.

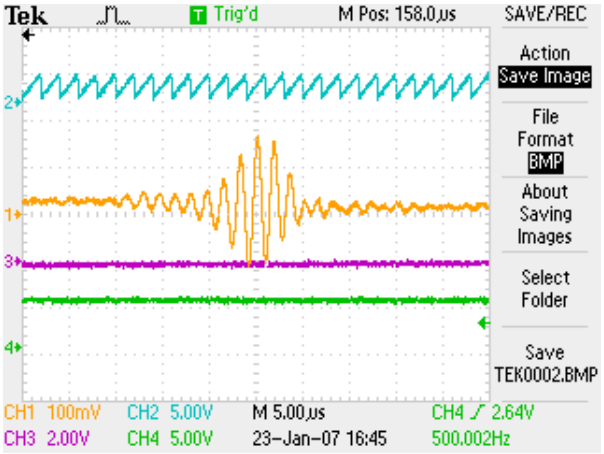

Figure 6.5: Interference Fringes (Smaller Time Scale)

To finally test the probe an image of a mirror has been done (picture 6.6). Because there is no transverse scanning (only a depth scan) the picture represents just a line. The representation is in black and white. Lighter is the pixel, more stronger the light is reflected or backscattered.

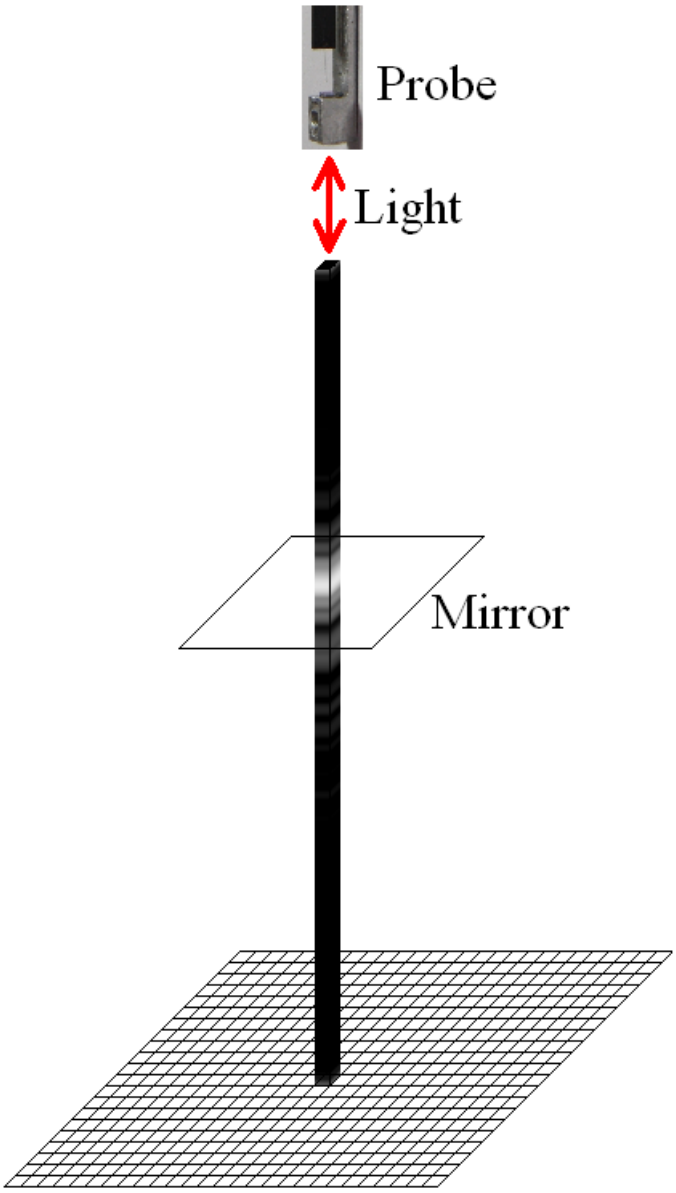

Figure 6.6: Depth Scanning (A-Scan) without Transverse Scanning

Chapter 7

Discussion

7.1 Bilaminar Axis

7.1.1 Resonance Frequency

The amplitude at the first resonance frequency is really different between the two experiments. The amplitude is bigger when the system is fixed in both sides.

The reason is that this frequency of 180 Hz is probably the resonance frequency of the system piezzo element fixed in cantilever and fibre sticked on. When the mechanical support is blocked on one side, it is able to move and therefore acting like an attenuator. But when it is not able to move laterally (like it is going to be in the whole system), the amplitude of the piezzo element reaches its maximum and it is not attenuated.

The amplitude of the beam at the second frequency (1160 Hz) is quite similar in both situations. That means this frequency is the optical fibre cantilever resonance frequency. This frequency is nearly twice lower than the theoretical one.

The parameters in the equation 5.1 page 21, can not vary a lot (values of table or theoretical values) except for the radius of the cantilever and the length. The length of the cantilever was measured with a micrometer and even in the worst cases ($\pm$ 0.2 mm), it is not possible to have a resonance frequency divide by two. Before sticking the fibre, a study of its diameter was completed with a microscope to check the quality of the stretching. Because the fibre was stretched by hand, the diameter could vary in order of $\pm 5\mu$m on the cantilever length but it is not enough to divide by two the resonance frequency.

The piezzo element is recovered with a protective layer which is very smooth and can possibly affect the resonance frequency like the material of the glue and the quality of the collage.

All these factors must act on this result and many other experiments have to be done, changing each parameters to understand perfectly the phenomenon.

7.1.2 Interferences Capability

The proof is established that this system is able to get interferences and therefore be used as a OCT probe. The problem is that the intensity of the light is just sufficient to interfere with a mirror as sample. This intensity can perhaps be enough to do pictures of the hard

tissues of the teeth but it is surely not strong enough to be used and get information on the soft tissues which have a much higher absorption coefficient. To improve the power of the output light it is really necessary to decrease the losses. These losses are due to several factors. One of them is the weld between the two optical fibres. Another is the fibre tip which is not so flat and perfectly cut as it has to be. A special tool must be found to cut fibres with a smaller outside diameter than standard one and therefore decrease the speckles. Because the fibre has been stretched it would decrease its ability to drive the light. The quality of the fibre may also be responsible and a higher quality of fibre should be chosen than a real standard one.

In the other hand to increase the power of the light in output, it would be possible to have a more powerful input light source. But even with a better light source a particular attention should be done to really decrease the losses.

The calculated focal distance is the same as the measured one and means that the fibre tip is on the right place before the lens.

Chapter 8

Conclusion

The mechanical part can not be tested as well as expected and the optical part shows some trouble but also some promising results. The fact is that after some experiments the design seems to be thought to perfectly and too rigid. This fact let not enough chances to give some corrections. The choice of the materials used can surely be improved to fit better the requirements. At least it is true that much more experiments have to be done to find out all the weak points of this design. But already many improvements can be realized to allowed more possibilities to adjust the system.

The OCT probes need many knowledges and experience in different fields and it would be really arrogant to believe that only one person with his first prototype could get the final product. But this prototype is a good departure point to develop, test and get a 3-D dental scanning imaging probe which can be put on the market.

This work allowed me to enlarge my knowledges in many field like mechanics, optics and dentistry. It let me discover the optical coherence tomography systems and probes. It also gave me the chance to work in a foreign country with other people who have others skills and way of thinking than mine. I had the possibility to do every steps of a system development and win a precious experience for my future professional and private life.

Hangzhou, China, February 15, 2007

Dubosson Fabrice
Rte de Croix-du-Nant 9,
1872 Troistorrents VS, Switzerland
dubosson.fabrice@gmail.com

Bibliography

[1] Online : http://www.answers.com.

[2] C. K. Hitzenberger A. F. Fercher, W. Drexler and T. Lasser. *Optical coherence tomography: principles and applications*, chapter 66, pages 239–303. INSTITUTE OF PHYSICS PUBLISHING, 2003.

[3] U. S. Sathyam L. B. DaSilva B. W. Colston, Jr. and L. L. Otis M. J. Everett, P. Stroeve. Dental oct. *OPTICS EXPRESS*, 3:230–238, September 1998.

[4] Brett E. Bouma and Guillermo J.Tearney. *Handbook of Optical Coherence Tomography*. Harvard Medical School and Wellman Laboratories of Photomedicine Massachussetts General Hospital Boston, Massachussetts, 2002.

[5] V. M. Gelikonov R. R. Iksanov R. V. Kuranov A. M. Sergeev N. D. Gladkova M. N. Ourutina J. A. Warren Jr. D. H. Reitze F. I. Feldchtein, G. V. Gelikonov. In vivo oct imaging of hard and soft tissue of the oral cavity. *OPTICS EXPRESS*, 3(6):239–250, September 1998.

[6] David Huang. *Optical Coherence Tomography*. PhD thesis, Massachusetts, May 1993.

[7] Felix P. Kapron. Geometrical optics of parabolic index-gradient cylindrical lenses. *Optical Society of America*, 60(11):1433–1436, November 1970.

[8] A. B. Coppens L. E. Kinsler, A. R. Frey and J. V. Sanders. *Fundamentals of Acoustics*. New York, 1982.

[9] Gaillard Mathieu. Conception et réalisation d'un cathéter pour des applications en imagerie médicale. Master's thesis, Unknown School in Lausanne Switzerland, 2005.

[10] LB DaSilva et al. MJ Everett, BW Colston. Fiber optic-based optical coherence tomography (oct) for dental applications. Proc SPIE 3489:53-59, 1998.

[11] Frederic Truffer. Line focus fourier domain optical coherence tomography. Diploma Work, April 2004. HEVs.

[12] Y. C. Chen M. J. Cobb X. D. li, X. M. Liu and M. B. Kimmey. Development of a fast scanning miniature probe and methods of dispersion management for high-resolution optical coherence tomography. In *26th Annual International Conference of the IEEE EMBS San Francisco, CA, USA*, September 2004.

Appendix A

The First Sketches

Here are the first ideas which are not be developed. They have been evaluated to choose the one which has been completed. The next table on page 35 will give the selection criteria, the coefficients and the results.

First idea, using a 2 axis Micro Electro Mechanical Systems (MEMS) to complete the scanning.

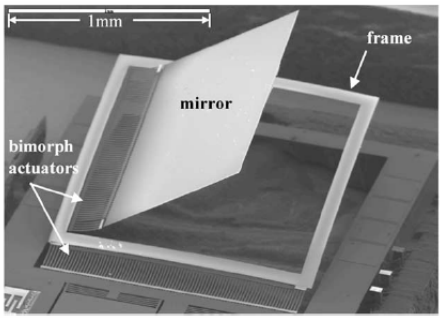

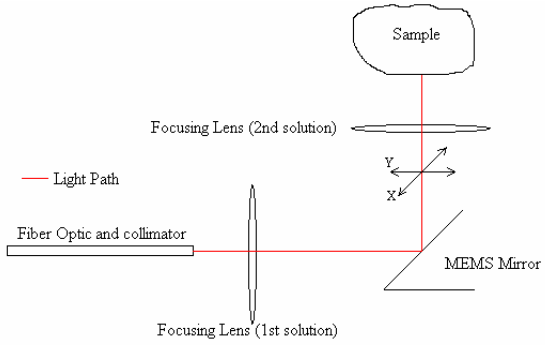

The second was to use an array of optical fibres. The scanning will be done in switching from fiber to fiber.

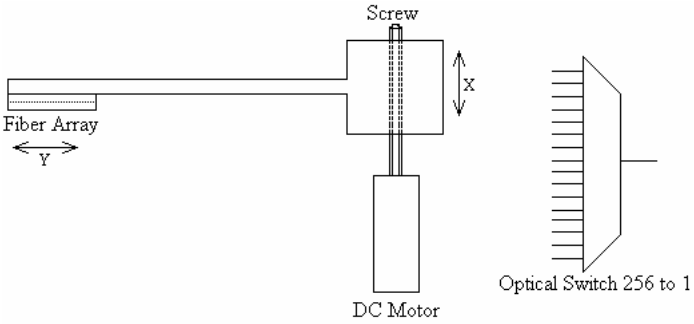

In the next idea the probe has to permanent magnets and two coils. In alimenting the coils magnetic fields are created and are able to displace the beam on the two axis.

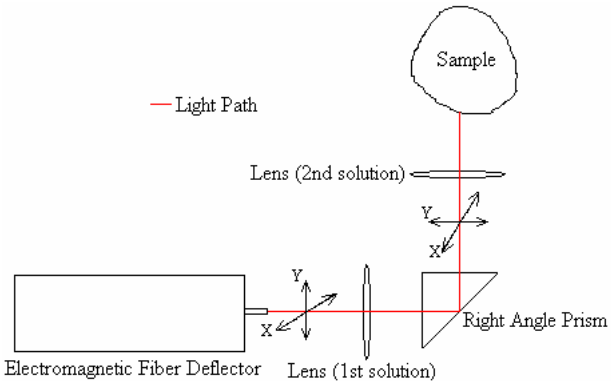

The following idea approaches the one developed in this report. Actually the second axis is not scanned in a translational way but the mirror rotate and give a polar representation of the sample.

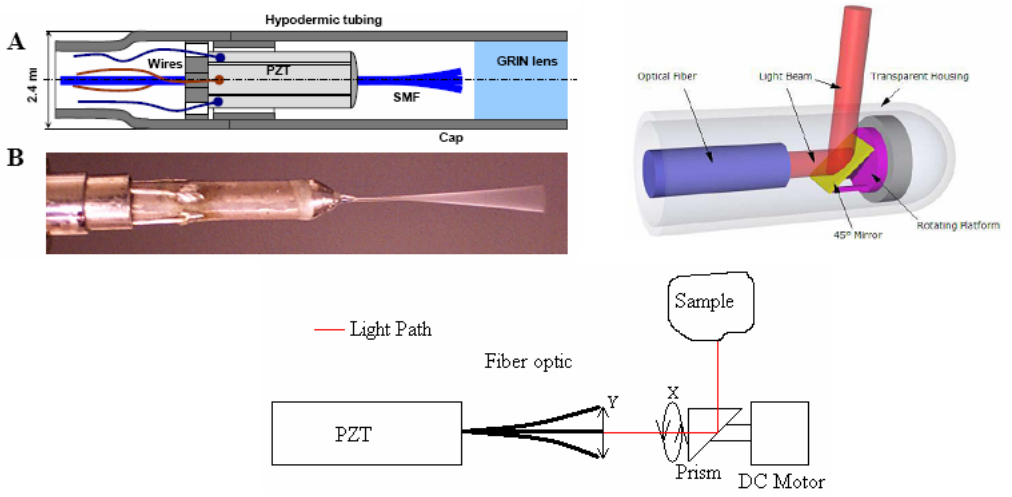

This possibility is directly control the mirror by the piezzo element and therefore doing the scanning.

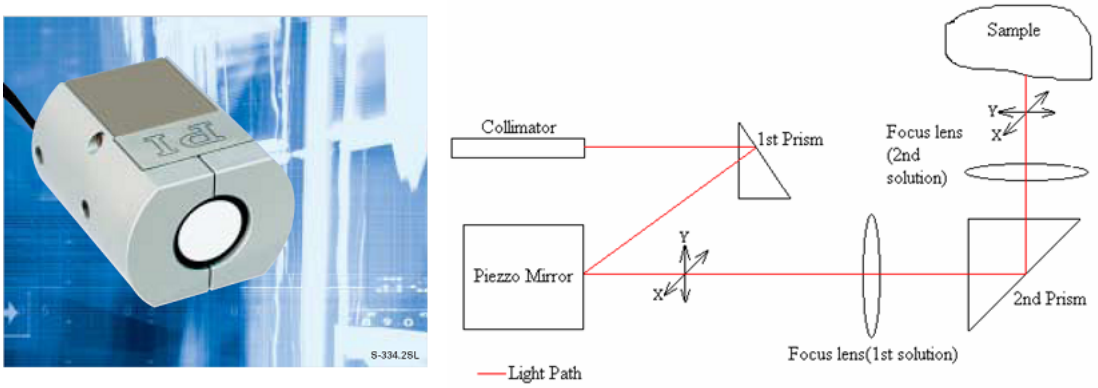

The last solution is scan the two axis with a DC Motor per axis.

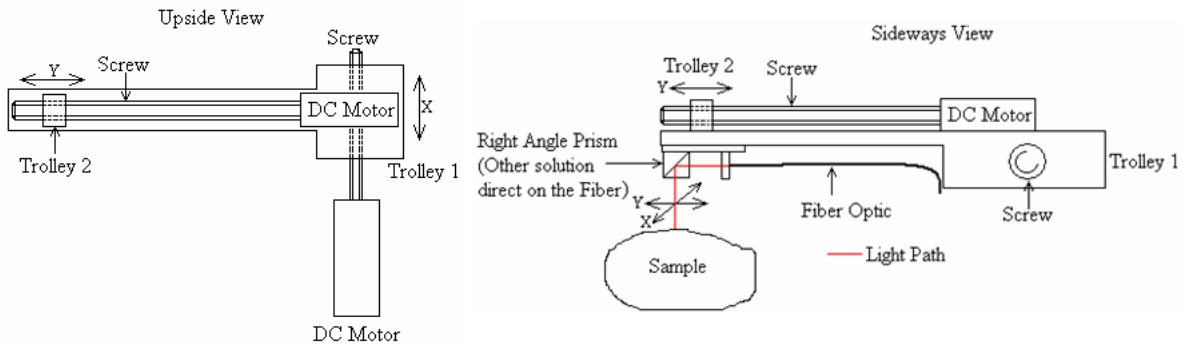

Here is the evaluation table. The second solution has been preferred because its higher scanning speed capacity allows it to be compatible with future OCT systems like Fourier domain OCT system.

Scanning probe	Safety	Sterizability	Convenience in application	Optical complexity	Mechanical complexity	Electrical complexity	Availability
Coefficient 1 to 10	10	10	7	5	3	5	8
MEMS	4	5	5	2	4	1	0
Fiber Array	5	5	3	2	3	3	3
Electromagnetic	4	5	3	3	2	1	0
PZT and Rotary Mirror	3	5	4	2	2	3	2
Piezo Mirror	3	5	2	2	4	3	4
PZT and Mechanical Axis	3	5	4	3	4	4	4
2 Mechanical Axis	5	5	3	4	3	5	5

Scanning probe	Cost	Scanning time	Patient comfort	Accessibility
Coefficient 1 to 10	10	8	7	8
MEMS	2	3	5	5
Fiber Array	0	4	4	5
Electromagnetic	2	3	3	3
PZT and Rotary Mirror	2	4	5	5
Piezo Mirror	2	3	3	4
PZT and Mechanical Axis	4	4	4	5
2 Mechanical Axis	4	2	4	4

Scanning probe		Result
Coefficient 1 to 10		
MEMS	"5"	271
Fiber Array	"7"	319
Electromagnetic	"6"	226
PZT and Rotary Mirror	4	282
Piezo Mirror	3	284
PZT and Mechanical Axis	2	327
2 Mechanical Axis	1	331

Appendix B

List of Instruments

- 2 oscilloscopes: Tektronix, TDS 2024, S/N: C033184; Tektronix, TDS 1012, S/N: 37617
- 3 functions generators: Stanford Research Systems, DS 345, S/N: 37617, 37618, 37619;
- 1 low noise preamplifier: Standford Research Systems, SR 560, S/N: 69010;
- 1 light source: BW Tek, BWC-SLD1B, λ 1200-1400 nm, S/N: 030602151;
- 1 laser: NEC, Module Nb GL 65320, $\lambda = 632.8$ nm, S/N: 533;
- 2 DC supply 0-30V;
- 1 optical fibres coupler 2×2, 50/50: S/N: SWCS-WIC1-22A 04090001A
- 1 polarization controller: Newport, F-POL-APC;
- 1 polarization controller: Fiberpro, IPC, S/N: 114336 A 081;
- 1 current amplifier: HCA-2M-1M, S/N: 02-03-018;
- 1 modulator: JDS Uniphase, S/N: 445942M;
- 1 galvanometer: diploma work;
- 1 acquisition card: National Instrument, BNC 2110, S/N: 1084651;
- optical fibres: single mode standard fibres;
- 1 personal computer.

Appendix C

GRIN lens

C.1 Company

FEMTO TECH. CO., LTD.
Add: 18 Development Road ChangAn High Tech. Park, Xian
Postcode:710119
Tel: +86-029-85691719
Fax: +86-029-85691717
http://feteco.com

C.2 Datasheet

Lot No.: G-20060213L268D365
Spec.: ZGR-18-23-1310-00-AR2
Diameter: 1.8 mm +0.005/-0.01 mm
Z-axis: 4.43mm +0.00/-0.04 mm
Pitch: 0.23P
Perpendicularity: 90° +/-20'
AR-Coating: R<0.5%@1310 nm +/-40 nm
$\sqrt{A}$: 0.3276@1310 nm
N0: 1.5940@1310 nm

Appendix D

DC Motor A max 16, Num. 110078

maxon A-max

A-max 16 ∅16 mm, Graphite Brushes, 2 Watt

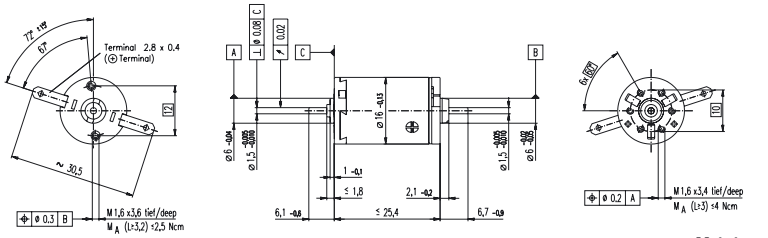

Stock program
Standard program
Special program (on request!)

Order Number	110071	110072	110073	110074	110075	110076	110077	110078	110079	110080
Motor Data										
1 Assigned power rating W	2.0	2.0	2.0	2.0	2.0	2.0	2.0	2.0	2.0	2.0
2 Nominal voltage Volt	2.4	3.6	6.0	12.0	12.0	15.0	18.0	18.0	24.0	36.0
3 No load speed rpm	16800	14300	9730	16000	11900	12800	13700	11300	13500	13300
4 Stall torque mNm	8.01	5.43	4.02	6.43	4.76	5.15	5.44	4.47	5.12	4.84
5 Speed / torque gradient rpm / mNm	2180	2760	2560	2590	2630	2600	2630	2670	2750	2880
6 No load current mA	187	103	39.1	35.2	24.7	21.5	19.4	15.5	14.3	9.38
7 Starting current mA	6120	2370	721	934	519	482	453	310	315	196
8 Terminal resistance Ohm	0.392	1.52	8.32	12.8	23.1	31.1	39.7	58.0	76.2	183
9 Max. permissible speed rpm	11900	11900	11900	11900	11900	11900	11900	11900	11900	11900
10 Max. continuous current mA	720	720	490	392	294	254	224	186	162	104
11 Max. continuous torque mNm	0.76	1.46	2.53	2.51	2.5	2.51	2.49	2.48	2.44	2.38
12 Max. power output at nominal voltage mW	3390	1950	975	2620	1430	1660	1880	1270	1740	1620
13 Max. efficiency %	67	63	59	65	61	63	63	61	62	61
14 Torque constant mNm / A	1.31	2.29	5.57	6.88	9.17	10.7	12.0	14.4	16.3	24.7
15 Speed constant rpm / V	7290	4170	1720	1390	1040	893	795	663	587	387
16 Mechanical time constant ms	24	24	23	23	23	23	23	23	23	24
17 Rotor inertia gcm²	1.05	0.816	0.864	0.854	0.844	0.854	0.848	0.834	0.811	0.788
18 Terminal inductance mH	0.02	0.05	0.31	0.47	0.83	1.13	1.42	2.05	2.61	6.01
19 Thermal resistance housing-ambient K / W	30	30	30	30	30	30	30	30	30	30
20 Thermal resistance rotor-housing K / W	5.5	5.5	5.5	5.5	5.5	5.5	5.5	5.5	5.5	5.5
21 Thermal time constant winding s	4	3	4	3	3	3	3	3	3	3

Specifications

- Axial play 0.05 - 0.15 mm
- Max. **sleeve bearing** loads
  axial (dynamic) 0.8 N
  radial (5 mm from flange) 1.4 N
  Force for press fits (static) 35 N
  (static, shaft supported) 280 N
- Max. **ball bearing** loads
  axial (dynamic) 2.2 N
  radial (5 mm from flange) 7.8 N
  Force for press fits (static) 30 N
  (static, shaft supported) 280 N
- Radial play **sleeve bearing** 0.012 mm
- Radial play **ball bearing** 0.025 mm
- Ambient temperature range -30 ... +85°C
- Max. rotor temperature +125°C
- Number of commutator segments 7
- Weight of motor 22 g
- 2 pole permanent magnet
- Values listed in the table are nominal.
  For applicable tolerances see page 43.
  For additional details please use the maxon selection program on the enclosed CD-ROM.

- Options: Ball bearings in place of sleeve bearings and pigtails in place of terminals.

Operating Range

Comments Details on page 49

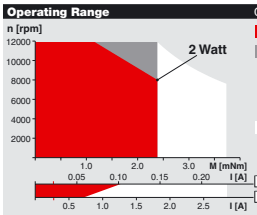

Recommended operating range

Continuous operation
In observation of above listed thermal resistances (lines 19 and 20) the maximum permissible rotor temperature will be reached during continuous operation at 25°C ambient.
= Thermal limit.

Short term operation
The motor may be briefly overloaded (recurring).

110080 Motor with high resistance winding
110071 Motor with low resistance winding

maxon Modular System

Overview on page 17 - 21

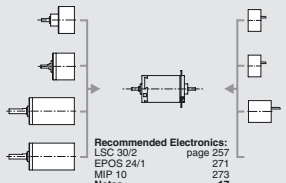

Spur Gearhead
∅16 mm
0.015 Nm
Details page 201

Spur Gearhead
∅16 mm
0.01 - 0.1 Nm
Details page 202 / 203 / 204

Planetary Gearhead
∅16 mm
0.1 - 0.3 Nm
Details page 205

Planetary Gearhead
∅16 mm
0.06 - 0.18 Nm
Details page 206

Recommended Electronics:
LSC 30/2 page 257
EPOS 24/1 271
MIP 10 273
Notes 17

Encoder MR
32 CPT,
2 / 3 channels
Details page 235

Encoder MR
128 / 256 / 512 CPT,
2 / 3 channels
Details page 236

Encoder MEnc
∅13 mm
16 CPT, 2 channels
Details page 251

April 2005 edition / subject to change

Appendix E

Encoder MR, Num. 201940

maxon tacho

Encoder MR, Type M, 128 - 512 Counts per turn, 2 / 3 Channels, with Line Driver

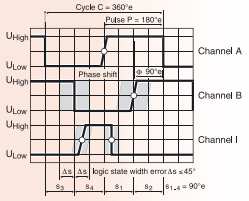

Stock program
Standard program
Special program (on request!)

Order Number	228179	228177	228181	228182	201937	201940
Type						
Counts per turn	128	128	256	256	512	512
Number of channels	2	3	2	3	2	3
Max. operating frequency (kHz)	80	80	160	160	320	320

Combination

+ Motor	Page	+ Gearhead	Page	+ Brake	Page	Overall length [mm] / ● see: + Gearhead					
RE 16, 3.2 W	74					45.4	45.4	45.4	45.4	45.4	45.4
RE 16, 3.2 W	74	GP 16, 0.1 - 0.3 Nm	205			●	●	●	●	●	●
RE 16, 3.2 W	74	GP 16, 0.06 - 0.18 Nm	206			●	●	●	●	●	●
RE 16, 4.5 W	76					48.4	48.4	48.4	48.4	48.4	48.4
RE 16, 4.5 W	76	GP 16, 0.1 - 0.3 Nm	205			●	●	●	●	●	●
RE 16, 4.5 W	76	GP 16, 0.06 - 0.18 Nm	206			●	●	●	●	●	●
A-max 16	102/104					30.4	30.4	30.4	30.4	30.4	30.4
A-max 16	102/104	GS 16, 0.015 Nm	201			●	●	●	●	●	●
A-max 16	102/104	GS 16, 0.01 - 0.1 Nm	202-204			●	●	●	●	●	●
A-max 16	102/104	GP 16, 0.1 - 0.3 Nm	205			●	●	●	●	●	●
A-max 16	102/104	GP 16, 0.06 - 0.18 Nm	206			●	●	●	●	●	●
A-max 19	106					34.0	34.0	34.0	34.0	34.0	34.0
A-max 19	106	GP 19, 0.1 - 0.3 Nm	207			●	●	●	●	●	●
A-max 19	106	GP 22, 0.5 - 2.0 Nm	211/212			●	●	●	●	●	●
A-max 19	106	GS 24, 0.1 Nm	215			●	●	●	●	●	●
A-max 19	108					35.8	35.8	35.8	35.8	35.8	35.8
A-max 19	108	GP 19, 0.1 - 0.3 Nm	207			●	●	●	●	●	●
A-max 19	108	GP 22, 0.5 - 2.0 Nm	211/212			●	●	●	●	●	●
A-max 19	108	GS 24, 0.1 Nm	215			●	●	●	●	●	●
A-max 22	110/112					36.9	36.9	36.9	36.9	36.9	36.9
A-max 22	110/112	GP 22, 0.1 - 0.6 Nm	209/210			●	●	●	●	●	●
A-max 22	110/112	GP 22, 0.5 - 2.0 Nm	211/212			●	●	●	●	●	●
A-max 22	110/112	GS 24, 0.1 Nm	215			●	●	●	●	●	●
RE-max 17	132/134					30.4	30.4	30.4	30.4	30.4	30.4
RE-max 17	132/134	GP 16, 0.1 - 0.3 Nm	205			●	●	●	●	●	●
RE-max 17	132/134	GP 16, 0.06 - 0.18 Nm	206			●	●	●	●	●	●
RE-max 21	136					34.0	34.0	34.0	34.0	34.0	34.0
RE-max 21	136	GP 22, 0.5 - 2.0 Nm	211/212			●	●	●	●	●	●
RE-max 21	136	GS 38, 0.1 - 0.6 Nm	223			●	●	●	●	●	●
RE-max 21	138					35.8	35.8	35.8	35.8	35.8	35.8
RE-max 21	138	GP 22, 0.5 - 2.0 Nm	211/212			●	●	●	●	●	●
RE-max 21	138	GS 38, 0.1 - 0.6 Nm	223			●	●	●	●	●	●
RE-max 24	140/142					36.9	36.9	36.9	36.9	36.9	36.9
RE-max 24	140/142	GP 22, 0.5 - 2.0 Nm	212			●	●	●	●	●	●
RE-max 24	140/142	GS 38, 0.1 - 0.6 Nm	223			●	●	●	●	●	●

Technical Data

Supply voltage V_{CC}	5 V ± 5 %
Output signal	TTL compatible
Index pulse width (nominal)	90°e
Operating temperature range	-25 ... +85°C
Moment of inertia of code wheel	≤ 0.09 gcm²
Output current per channel	max. 5 mA

Attention: The index signal I is synchronised with channel A or B.

Pin Allocation

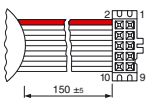

1	Motor +
2	V_{CC}
3	GND
4	Motor –
5	Channel $\overline{A}$
6	Channel A
7	Channel $\overline{B}$
8	Channel B
9*	Channel $\overline{I}$ (Index)
10*	Channel I (Index)

DIN Connector 41651
flat band cable AWG 28
* version with 3 channels

Connection example

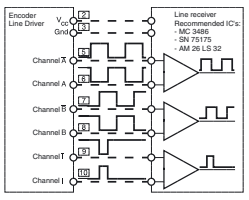

Appendix F

Positionning Control Unit, EPOS 24/1

maxon motor control

EPOS Positioning Control Units

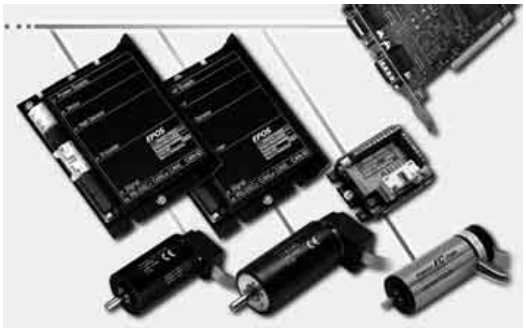

Advantages	Features
• Digital	Digital position-, speed- and current-control
• Flexible, modular	Versions for brush and brushless DC drives, from the smallest micro-drive up to 700 Watt motors.
• Extendable	Networking of up to 127 drive units in one CAN Bus
• Easy start-up procedure	Cable available. Numerous prepared IEC-1131 libraries for CAN Master units, Windows DLL for RS232 and PC-CAN card with several programming examples, support through Graphical User Interface, start-up wizard, diagnosis help, automatic regulator turning.
• Standardised	CANopen standard CiA DS-301 and DS-402 Broad spectrum of controllers, I/O modules and controllers of third-party suppliers available that can easily be used with EPOS.
• Excellent price / performance ratio	Cutting-edge technology helps provide wide-ranging sophisticated functionality, sinusoidal commutation for the lowest torque ripple in EC motors. Motor chokes are already built into EPOS.

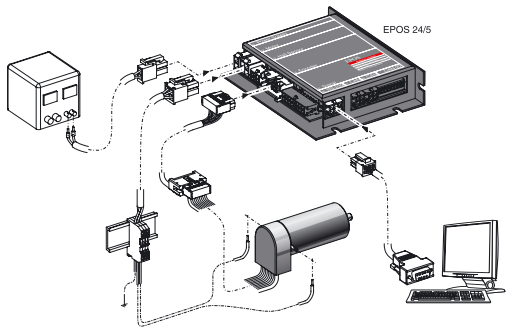

Function description
EPOS is a modular-designed digital positioning system suitable for DC and EC motors with incremental encoder. The performance range of these compact positioning controllers starts at a few watts and goes up to 700 W.

A variety of operating modes means that all kinds of drive and automation systems can be flexibly assembled using positioning, speed and current regulation. The built-in CANopen interface allows networking to multiple axis drives, with additional I/O modules and online commanding by CAN Bus master units.

- CANopen profile position-, profile velocity- and homing mode
- Position-, velocity- and current-mode
- Sinusoidal or trapezoid path generator
- Velocity and acceleration feed forward
- Digital position reference by Pulse/ Direction or master encoder
- Sinusoidal or Trapezoid Commutation for EC motors
- Smart multi-purpose digital I/O's configurable as: Positive and negative limit switches, Home switch, Brake output
- General purpose digital I/O's and analogue inputs
- Communication through CAN and/or RS-232
- Gateway RS232 to CAN
- Windows-based Graphical User Interface for set-up, start-up and auto-tuning

Extensive software assistance and a Graphic User Interface support the start-up procedure, regulator adjustment and adapting to the PC world or other CANopen equipment.

Available documentation and software
- Getting Started
- Cable Starting Set
- Hardware Reference
- Graphical User Interface (GUI)
- Windows DLL
- IEC1131 Libraries
- Firmware Specification
- Communication Guide
- Application Notes
- Application Samples

Cable accessories (option)
A comprehensive range of cables is available as an option.
Details can be found on page 275.

EPOS 24/1

DIGITAL CANopen RS232 GUI

Matched with DC brush motors with encoder or brushless EC motor with Hall sensors and encoder up to 20 Watt.

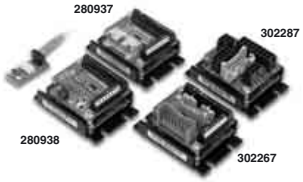

EPOS 24/5

Matched with DC brush motors with encoder or brushless EC motors with Hall sensors and encoder, from 5 to 120 Watt.

EPOS 70/10

Matched with DC brush motors with encoder or brushless EC motors with Hall sensors and encoder, from 80 to 700 Watt.

Order numbers

280937	EPOS 24/1 for DC motors
280938	EPOS 24/1 for EC 6 motor
302267	EPOS 24/1 for EC 16 / EC 22 motors
302287	EPOS 24/1 for DC / EC motors
275512	EPOS 24/5
300583	EPOS 70/10

Accessories

309687	Shunt regulator (EPOS 24/1 and 24/5)
235811	Shunt regulator (EPOS 70/10)

Mechanical data

- Weight
  - EPOS 24/1: approx. 45 g
  - EPOS 24/5: approx. 170 g
  - EPOS 70/10: approx. 330 g
- Dimensions (L x W x H)
  - EPOS 24/1: 55 x 40 x 25 mm
  - EPOS 24/5: 105 x 83 x 24 mm
  - EPOS 70/10: 150 x 93 x 27 mm
- Mounting plate: Flange for M3-screws

Electrical Data

- Supply voltage V_{CC} (Ripple < 10%)
  - EPOS 24/1: 9 - 24 VDC
  - EPOS 24/5: 11 - 24 VDC
  - EPOS 70/10: 11 - 70 VDC
- Max. output voltage
  - EPOS 24/1: 0.98 x V_{CC}
  - EPOS 24/5: 0.9 x V_{CC}
  - EPOS 70/10: 0.9 x V_{CC}
- Max. output current I_{max} (<1 s)
  - EPOS 24/1: 2 A
  - EPOS 24/5: 10 A
  - EPOS 70/10: 25 A
- Continuous output current I_{cont}
  - EPOS 24/1: 1 A
  - EPOS 24/5: 5 A
  - EPOS 70/10: 10 A
- Sample rate of PI - current controller: 10 kHz
- Sample rate of PI - speed controller: 1 kHz
- Sample rate of PID - positioning control: 1 kHz
- Max. speed (motor with 2 poles): 25 000 rpm
- Built-in motor choke per phase
  - EPOS 24/1: 150 µH / 1 A (DC / EC motors); 300 µH / 0.7 A (EC 6 motor)
  - EPOS 24/5: 15 µH / 5 A
  - EPOS 70/10: 25 µH / 10 A

Inputs

- Hall sensor signals: H1, H2, H3
- Encoder signals: A, A\, B, B\, I, I\ (max. 1 MHz)
- Digital inputs
  - EPOS 24/1: 6 digital inputs
  - EPOS 24/5: 6 digital inputs
  - EPOS 70/10: 8 digital inputs
- 2 analogue inputs: 10-bit resolution, 0 … +5 V
- CAN-ID (CAN node identification)
  - EPOS 24/1: configurable with DIP Switch 1 … 4
  - EPOS 24/5: configurable with DIP Switch 1 … 7
  - EPOS 70/10: configurable with DIP Switch 1 … 7

Outputs

- Digital outputs
  - EPOS 24/1: 2 digital outputs
  - EPOS 24/5: 4 digital outputs
  - EPOS 70/10: 4 digital outputs

Voltage outputs

- Encoder supply voltage: +5 VDC, max 100 mA
- Hall sensor supply voltage: +5 VDC, max. 30 mA
- Auxiliary supply voltage
  - EPOS 24/1: +5 VDC, max. 10 mA
  - EPOS 24/5: V_{CC}, max. 1300 mA
  - EPOS 70/10: +5 VDC (R_i = 1 kΩ)

Interface

- RS232: RxD; TxD (max. 115 200 bit/s)
- CAN: high; low (max. 1 Mbit/s)

LED indicator

- LED
  - EPOS 24/1: red LED, green LED
  - EPOS 24/5: Bi-colour LED
  - EPOS 70/10: Bi-colour LED

green = READY, red = ERROR

Ambient temperature / humidity range

- Operation: -10 … +45°C
- Storage: -40 … +85°C
- No condensation: 20 … 80 %

Appendix G

Datasheet: Piezzo Element

Stripe Actuators

Dimensions (mm)			Free Length (mm)	Total Deflection (mm)	Blocking Force (N)	Resonance Frequency (Hz)	Capacitance (pF)
Long	Wide	Thick					
Catalog No. 40-1010 (600/200/0.60-SA)							
60.0	20.0	0.60	53	>2.5	>0.25	65	170,000
Catalog No. 40-1035 (490/018/0.60-SA)							
49.0	1.8	0.60	42	>1.5	>0.03	110	25,000
Catalog No. 40-1025 (490/021/0.60-SA)							
49.0	2.1	0.60	42	>1.5	>0.05	110	15,000
Catalog No. 40-1040 (400/200/0.60-SA)							
40.0	20.0	0.60	33	>1.0	>0.40	175	115,000
Catalog No. 40-1055 (350/025/0.60-SA)							
35.0	2.5	0.60	28	>0.7	>0.06	245	12,000

Deflections and blocking forces measured at driving voltage of 150 V (maximum) in direction of polarization.
Operating temperature: -25°C to 70°C; storage temperature: -40°C to 85°C.

Stripe Actuator: Better Performance and Longer Lifetime

- Superior layering technology, for
  greater range of deflection
  useful blocking forces
- Varnish layer protects surface from humidity and dust

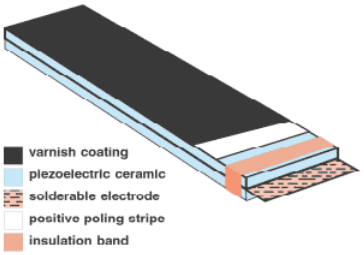

- Proprietary layering technology increases flexibility, allows greater deflection
- Parallel electrical configuration of ceramic layers ensures high sensitivity to input; compatible with bias voltage circuitry that eliminates the potential for depolarizing the ceramic layers
- Varnish layer electrically insulates surface, protects from humidity, dust, other hazards
- White stripe identifies positive surface
- Solderable electrode bonded between plates
- Thickness tolerance for part without applied coatings

Advanced layering technologies have enabled APC International, Ltd. to develop the Stripe actuator, a flexing actuator that achieves greater deflections than conventional designs. Stripe actuators derive their name from a white stripe that denotes the positive surface.

A standard sized Stripe actuator secured in a cantilever mounting configuration has a deflection range of up to >2.5 mm, in response to a 150 V (maximum) input. If deflection is blocked, a Stripe actuator will develop a useable force. The relationships discussed in technical note *Performance of Stripe Actuators* determine the deflections and blocking forces for these actuators.

Variables Affecting the Performance of a Stripe Actuator

a	dimensions	total length (ltot) free length (lf) width (w) thickness (h)
b	deflection	
c	cantilever mounting: bonded attachment	
d	cantilever mounting: point attachment	
e	parallel drive	(high sensitivity to input) 50 V max
f	bias drive	(eliminates potential for depolarization) 150 VDC bias max.

Performance of Stripe Actuators

Note that for all standard Stripe actuators thickness (h) is 0.60 mm.

Characteristic	Calculation	Result
Total Deflection	$2.2 \times 10^{-6} \times ([l_f]^2 / [h]^2) ([V])$	[ ] mm
Compliance	$26.4 \times 10^{-5} \times ([l_f]^3 / ([w]) ([h]^3))$	[ ]
Blocking Force	[deflection] / [compliance]	[ ] N
Resonance Frequency	$3.2 \times 10^5 \times ([h] / [l_f]^2)$	[ ] Hz

l_f = free length of actuator
h = thickness of actuator (0.60 mm is standard)
w = width of actuator
V = voltage (150 V maximum)

http://www.americanpiezo.com/

Appendix H

Physic Parameter of the Optical Fiber

Fibercore Limited, Chilworth, SO16 7QQ, UK **Factnote 4.1.2**	FIBERCORE LIMITED
The Physical Properties of Silica and UV Cure Acrylate Coating Packages	**Page 1 of 1** **June 2004**

This Factnote provides you with a range of physical parameters for fused silica, in addition to selected parameters for 10mol% borosilicate which is representative of the composition of 'bow-ties' themselves. It is intended to help you model the behaviour of Fibercore fibers. In the majority of situations, the fused silica values will be adequate because the bulk of most of our fibers is composed of this material. The values for borosilicate relate only to the bow-ties of HiBi fibers.

	Silica		**Borosilicate**
Refractive index at 633nm	1.457		1.446
Thermal expansion coefficient	5.5×10^{-7}°C^{-1}		14×10^{-7}°C^{-1}
Density		2.2gcm^{-3}	
Change in refractive index with temperature (0-700°C)		8.6×10^{-4}%°C^{-1}	
Thermal conductivity (100°C)		0.0033 calcm^{-1}S^{-1}°C^{-1}cm^{-1}	
Verdet constant		1.56×10^{-2} minA^{-1}	
Stress-optic coefficient		8.72×10^{-10}m^{2}N^{-1}	
Kerr coefficient		2×10^{-15}m/V	
Young's modulus	10.4×10^6psi		9.8×10^6psi
Change in Young's modulus with temperature (0-900°C)	0.01%°C^{-1}		0.01%°C^{-1}
Poisson's ratio	0.17		0.19

Fibercore use a generic dual acrylate coating package with the following key attributes.

Dual acrylate package for a 125 micron coated fiber – typical properties

Cured characteristics	**Primary Coating - Inner**	**Secondary coating - Outer**
Refractive index	1.57	1.54
Transition temperature	-20°C	55°C
Secant modulus (2.5% strain)	1.5MPa	750MPa
Elongation	150%	25%
Tensile strength	1.0MPa	28MPa
E' 1000 MPa*	-57°C	32°C
E' 100 MPa**	-35°C	55°C

* From the dynamic mechanical analysis curve (DMA) the temperature at which the secant modulus exceeds 1000MPa

** From the dynamic mechanical analysis curve (DMA) the temperature at which the secant modulus exceeds 100MPa

IF YOU NEED TO KNOW MORE
Tel: +44 (0)23 8076 9893 Fax: +44 (0)23 8076 9895
Email: Info@fibercore.com Website: www.fibercore.com

Appendix I

The Mechanical Drawings